UNIVERSITY OF BIRMINGHAM

Three-dimensional catalyst electrodes based on PtPd nanodendrites for oxygen reduction reaction in PEFC applications

Lu, Yaxiang; Du, Shangfeng; Steinberger-Wilckens, Robert

[Link to publication on Research at Birmingham portal](#)

Corresponding Author: Dr. Shangfeng Du, PhD

Corresponding Author's Institution: University of Birmingham

First Author: Yaxiang Lu

Order of Authors: Yaxiang Lu; Shangfeng Du, PhD; Robert Steinberger-
Wilckens

Dear Prof Xenophon E. Verykios and Reviewers,

Thank you for your time and your valuable comments. We have revised the manuscript carefully according to Reviewers' comments.

All major revisions were highlighted in the Revised Manuscript − Marked up. Please also find our responses to the comments point-by-point in the Response to Reviewers' comments.

In this paper, we demonstrated for the first time catalyst electrodes with PtPd nanodendrites for polymer electrolyte fuel cell (PEFC) applications. The originality and novelties of this work are listed as below:

1)   Direct catalyst electrode with PtPd nanodendrites. The PtPd nanodendrites themselves have been widely investigated in past decades. However, they are all focused on the pure materials research for fuel cell reactions, and none of them has been involved in the catalyst electrode of real fuel cells while which is the topic of this work. For the first time, we demonstrate the catalyst electrode from PtPd nanodendrites for PEFC applications in this work.

2)   In-situ growing PtPd nanodendrites on large-area carbon paper. The deposition of nanostructures on large-area direct component is highly preferred because they can be directly forwarded to application, but it's much more difficult than the synthesis in solution or nanoparticle surface, e.g. CNTs or graphene, and still remains as a challenge. In this work, this was successfully achieved. Uniformly distributed PtPd nanodendrites are directly grown on the 16 cm^2 gas diffusion layer carbon paper surface and used as PEFC catalyst electrodes.

3)   Direct evidences for the crystal growth mechanism. For PtPd nanodendrites, the crystal growth mechanism is usually inferred by their standard reduction potential in literature, and we provide more direct evidences here.

In this case, this work specially relates to the scope of journal on 'New catalytic routes and processes for the production of clean energy'.

We confirm that this manuscript has not been published elsewhere and is not under consideration by any other journals. All authors have approved the manuscript and agreed with this submission. The authors have no conflicts of interest to declare.

Thank you for considering our manuscript.

Sincerely yours,
Shangfeng Du

Centre for Hydrogen and Fuel Cell Research
School of Chemical Engineering, University of Birmingham, Birmingham B15 2TT, UK
E-mail: s.du@bham.ac.uk

Response to Reviewers

Dear Editor and Reviewer,

Thanks again for your time and your valuable comments for our revised manuscript. We've added one phrase in the text according to Reviewer's comments. Please find our response to the comment below:

Reviewer #1: *The authors have made significant improvement of the manuscript over the previous draft. One last question before recommending this work for publication. Based on the experimental description, it seems that the catalysts grow on both sides of the GDL. If so, which side of GDL do you use for MEA? Does the metal NPs on the other side affect the mass transfer of oxygen? This at least might be mentioned in the text.*

Response: The catalysts only grow on the topside with MPL which is the side facing the polymer electrolyte membrane in the membrane electrode assembly. Due to the hydrophobic feature of GDL, reaction solution does not penetrate into the pores of GDLs so all catalysts only grow on the MPL surface. We've added one phrase to clear this point on Page 5 in the text.

Three-dimensional catalyst electrodes based on PtPd nanodendrites for oxygen reduction reaction in PEFC applications

Yaxiang Lu, Shangfeng Du[*], Robert Steinberger-Wilckens

School of Chemical Engineering, University of Birmingham, Edgbaston, Birmingham B15 2TT, UK

To whom correspondence should be addressed to:

*SF Du: E-mail: s.du@bham.ac.uk, Tel: +44-121-4158696

Abstract

PtPd bimetallic nanodendrites (NDs), with enhanced activities from PtPd over element Pt and unique anisotropic morphology, show potential as catalysts in fuel cell applications. However, the research has been limited to pure materials, and constructing a practical fuel cell catalyst electrode from PtPd NDs still remains as a challenge. In this paper, we demonstrated, for the first time, catalyst electrodes from PtPd NDs for polymer electrolyte fuel cell (PEFC) applications. PtPd NDs are in-situ grown on large-area carbon paper gas diffusion layers (GDLs) and directly employed as cathodes in H_2/air PEFCs. The thin catalyst layer with PtPd nanodendrites significantly reduces mass transfer resistance and a higher power performance is achieved than those based on pure Pt nanowires and Pt/C nanoparticle electrocatalysts. The crystal growth mechanisms of this advanced nanostructure on large-area support are also detailed based on the time-dependent experiments and Pd content.

1. Introduction

Due to unique properties, one-dimensional (1D) nanostructures such as nanodendrites (NDs), nanowires (NWs) and nanotubes (NTs) have been widely studied for their enhanced catalytic activities toward fuel cell reactions [1-4]. Compared with associated zero-dimensional (0D) nanoparticles (NPs), 1D nanostructures have more enhanced reaction kinetics on catalyst surface and are less vulnerable to dissolution and aggregation, which can potentially improve their catalytic activity and durability [5-7]. Benefiting from these advantages, three-dimensional (3D) nanostructures based on 1D Pt nanowire arrays have been fabricated by bottom-up design and demonstrated as effective catalyst electrodes to address some challenges faced by the conventional fuel cell electrodes with Pt-based NPs [8, 9]. These 3D catalyst electrodes have been confirmed with high performance in real fuel cells owing to a high catalyst utilisation ratio resulted from a significantly reduced mass transfer resistance induced by the thin and porous catalyst layer, as well as unique catalytic properties of single-crystal Pt NWs [10-12].

Although Pt is still the best electrocatalyst for the oxygen reduction reaction (ORR) in cathodes for polymer electrolyte fuel cells (PEFCs), the relative high cost, and in particular the poor stability are still the major limits for the successful commercialization of this technology [13, 14]. In order to improve the stability and reduce the loading of precious Pt while not compromising the activity, one promising strategy is to introduce other element into Pt to form alloy or hybrid catalysts [15, 16]. It is generally accepted that the incorporation of a second metal component can offer desired interactions with Pt to tune both electronic and surface effects, triggering enhanced effects to improve physical and chemical properties [17, 18]. Sitting in the

3

same periodic group as Pt and possessing a similar lattice space, Pd has been confirmed as a promising candidate [19, 20]. 1D Pt-Pd bimetallic electrocatalysts with various structures such as alloy [21], core-shell [22] and heterostructure as well as different morphologies like nanodendrites [23, 24], nanowires [21], nanotubes [22], nanorods [25] etc. have been reported. The advantages of the bimetallic feature and 1D anisotropic properties lead to an improved catalysis process [26-28], resulting in a long-term stability and also superior activity toward ORR. Some references also indicated that the existence of Pd played a significant role on the morphology of Pt-Pd bimetallic nanostructures [28]. For example, Xia's group [23] reported that in the presence of Pd, open branched PtPd dendrites were formed, otherwise only foam-like Pt aggregates were obtained. However, these investigations all focus only on the pure material research, and the real applications of 1D Pt-Pd bimetallic catalysts in practical fuel cells still remains as a challenge.

Inspired by the 3D Pt-nanowire (PtNW) catalyst electrodes and considering the enhanced activity between Pd and Pt, in this work, direct catalyst electrodes with PtPd bimetallic NDs in-situ grown on 16 cm^2 gas diffusion layers (GDLs) are demonstrated. The crystal growth mechanism and influence of Pd on the PtPd nanostructure are studied based on the time-dependent in-situ growing process and the Pd content. The fabricated gas diffusion electrodes (GDEs) with 3D PtPd bimetallic nanostructures are directly tested as cathodes in H_2/air PEFCs. The polarization curves, electrochemical impedance spectra (EIS), cathode cyclic voltammograms (CVs) and accelerated degradation test (ADT) are performed in-situ in PEFCs to investigate the enhanced power performance and durability of PdPtND GDEs.

2. Experimental Section

2.1 Chemicals and materials

Hexachloroplatinic acid hexahydrate ($H_2PtCl_6 \cdot 6H_2O$, ≥37.50% Pt basis) and palladium(II) chloride ($PdCl_2$, anhydrous, 60% Pd basis) from Sigma-Aldrich UK were used as metal precursors. Formic acid (CH_2O_2, 98+%) and isopropanol (IPA) (C_3H_8O, >99.5%) were obtained from Fisher Scientific UK. DuPont Nafion® 212 membrane, Nafion® solution (D1021, 10 wt%) and SIGRACET® GDL 35 BC carbon paper were purchased from Ion Power Inc. 20 wt% Pt supported on Vulcan XC-72 was purchased from Fuel Cell Store. All chemicals and materials were used as received without any further purification. The GDL 35 BC carbon paper was used as the direct substrate for PtPd nanostructure growth. Gas diffusion electrodes (GDEs) with Pt/C catalysts at a loading of 0.4 mg_{Pt} cm^{-2} printed on SIGRACET® GDL 34 BC were obtained from Johnson Matthey Fuel Cells Ltd and used as anodes for fabricating single cells. Ultrapure water (18.2 MΩ cm) from a Millipore water system was used throughout.

2.2 PtPd GDE preparation and physical characterization

Pieces of 4×4 cm^2 standard GDL 35 BC carbon paper was used as the substrate. It consists of a carbon fibre layer at the back and a top micro porous layer (MPL) from carbon spheres with a particle size of 50–100 nm. The GDL has been treated with polytetrafluoroethylene (PTFE) to give super hydrophobic property to prevent the water flooding in fuel cell operation. PtPd nanostructures with various molar ratios were grown on carbon paper at MPL surface by a modified wet chemical reduction method from our previous studies [31]. In a typical synthesis, to ensure the total metal loading of 0.4 mg cm^{-2} on a 16 cm^2 carbon paper, a controlled amount of H_2PtCl_6 and

$PdCl_2$ solution coupled with 0.53 mL formic acid were added to 10.6 mL water. Then the carbon paper was immersed in the mixed solution at the bottom in a 6 cm glass Petri dish and stored at room temperature for PtPd nanostructure growth. After the colour of the solution changed from yellow to colourless and the growth process was completed, the samples were rinsed using water and IPA, followed by drying at 40 ^{o}C overnight. The as-prepared carbon paper samples with in-situ grown PtPd nanostructures at various Pd atomic percentages of 50, 25, 10, 5, 2.5 and 0.5 were directly used as GDEs at cathode for PEFCs.

The distribution and morphology of PtPd nanostructures in electrodes were characterized by a field emission scanning electron microscope (FE-SEM, JEOL 7000F, operating at 20 kV) and a high-resolution transmission electron microscope (HR-TEM, Philips CM200 FEG). TEM samples were prepared by scraping catalysts from GDE surface and dispersed onto Cu grids. X-ray diffraction (XRD) patterns were recorded with a Siemens D5005 powder X-ray diffractometer operated at 40 kV and 30 mA using Cu Kα (λ= 0.15418 nm) radiation. X-ray photoelectron spectroscopy (XPS) characterization was conducted on an XPS spectrometer (K-Alpha, Thermo Scientific) with a micro-focussed monochromatized Al Kα radiation.

2.3 Membrane electrode assembly (MEA) fabrication

Membrane electrode assemblies (MEAs) with an active area of 16 cm^2 were fabricated using the as-prepared PtPd GDEs as cathodes and the Pt nanoparticle GDEs from Johnson Matthey as anodes. GDEs were first coated with a thin layer of Nafion ionomer at a loading of 0.6 mg cm^{-2}, and then sandwiched at both sides of a 6×6 cm^2 Nafion 212 membrane. After that, the assembly was hot pressed at 125 ^{o}C

under a pressure of 4.9 MPa for 2 min. An illustration of the MEA setup is shown in Fig. 1. For comparison, MEAs with cathodes based on Pt/C (20 wt%) nanoparticle catalysts and pure Pt nanowires at a Pt loading of 0.4 mg_{Pt} cm^{-2} were also fabricated simultaneously.

2.4 Fuel cell tests

The fabricated MEAs were tested in a PEFC test stand (PaxiTech-BioLogic FCT-50S, Fig. 1) with electrochemical impedance spectroscopy (EIS) capabilities. The gasket used in fuel cell testing was PTFE sheet with a thickness of 254 μm at both cathode and anode sides. All tests were conducted at 70 ^{o}C with fully humidified H_2 and air fed at stoichiometry of 1.3/2.4 and backpressure of 2 bars at the anode and cathode, respectively. The MEAs were conditioned by a break-in at 0.6 V for 7 h, and after that polarization curves were recorded at a scan rate of 5 mV s^{-1} from 0.3 V to open circuit voltage (OCV). EIS measurements were performed in the frequency range from 10 kHz to 0.1 Hz with amplitudes of 0.05, 1 and 2 A at current densities of 0.05, 0.5 and 1 A cm^{-2} for 16 cm^2 PEFCs, respectively.

Cathode cyclic voltammograms (CVs) were recorded using an EZstat-Pro system integrated with the test stand. The cell temperature and backpressure were 25 ^{o}C and 0 bar, respectively. The cathode was fed with fully humidified N_2 at 300 mL min^{-1}, and the anode was fed with fully humidified pure H_2 at 120 mL min^{-1} serving as both reference and counter electrodes, also called a dynamic hydrogen electrode (DHE). Then the cathode potential was cycled between 0.05 and 1.2 V versus DHE at 20 mV s^{-1} for 5 cycles, and the fifth cycle was recorded. Accelerated degradation test (ADT)

was undertaken by potential cycling between 0.6 and 1.2 V for 3000 cycles at a scan rate of 50 mV s^{-1}.

3. Results and discussion

The controlled growth of PtPd nanostructures on 16 cm^2 GDLs was realized by reducing $H_2PtCl_6 \cdot 6H_2O$ and $PdCl_2$ with formic acid in aqueous solution at room temperature [29, 30]. The composition of PtPd nanostructures was tuned by the amount of precursors added in the reaction system while keeping the total metal loading at 0.4 mg cm^{-2}. Since the GDL surface consists of only the inert carbon spheres coated with hydrophobic PTFE, only limited rough sites of carbon sphere surface can serve as the main heterogeneous nucleation sites in the reduction. In our previous research it has also demonstrated that on this kind of surface, the edge area of GDL piece is usually easier to be wetted and provides more nucleation sites than the central region in an aqueous solution [11]. In this case, the population of Pt nuclei multiplies at the edge area while fewer are in the center; therefore more catalyst nanostructures are formed and accumulate at the edge of the GDL piece to form large agglomerates. Comparing with the standard reduction potential of $PtCl_6^{2-}$/Pt (0.73 V vs. standard hydrogen electrode (SHE)), the value for Pd^{2+}/Pd couple is more positive (0.92 V vs. SHE), meaning that Pd nuclei can form on the GDL surface much easier than Pt [28]. This relative positive standard reduction potential enables the generated Pd nanoparticles distribute more uniformly on the inert surface, which then act as seeds to induce the co-reduction and further growth of PtPd nanostructures [24, 32]. Fig. 2 compares the surface at the edge and center area of a 16 cm^2 PtNW GDE and PtPd GDE with 5 at% Pd. It can be seen that the distribution of PtPd nanostructures has much less difference at the edge and in the center area as compared to Pt.

Although the PtPd nanodendrites have been reported by many groups, including both in solutions [23, 28, 33] and on supports, e.g. on graphene [32, 34], the growth mechanism was all simply inferred based on the standard reduction potential. There is really not a lot of evidences for the crystal growth mechanism. To help clear this point, in this work, the time-dependent in-situ growing process was analysed for PtPd GDE with 5 at% Pd. The reaction solution from 0 to 92 hours was monitored by UV-Vis spectroscopy to evaluate qualitatively the remained metal ions which haven't been reduced by formic acid. The absorption spectrum lines of the Pd and Pt precursors as well as that of the PtPd mixture at different time intervals are shown in Fig. S1. The results indicate that the reduction of Pd mainly happens at the initial stage of the reaction and nearly all Pd ions are reduced in the first 2 hours, but the whole reaction, in particular the reduction of Pt will not finished until 24 hours later.

To further understand the crystal growth mechanism, the morphological evolution of PtPd nanostructure with 5 at% Pd on the GDL surface at various reaction periods were examined by TEM with EDX analysis (Fig. S2). The results show a very high Pd ratio in the beginning, followed by a fast dropping to a quite low level, suggesting that PtPd alloy nanoparticles with a dominated amount of Pd at the initial stage are formed at first, which are then working as seeds for the following growth to nanodendrites. The branches of nanodendrites are dominated by Pt due to most Pd has been reduced in the initial period in nanoparticle formation. These changes are consistent with that shown by UV-Vis spectra. The branch diameter of the as-obtained nanodendrites is ca. 4 nm, and the length is ca. 5–20 nm. The crystalline nature of final PtPd nanodendrites was elucidated by the selected-area electron diffraction

9

(SAED) pattern, and intense rings can be assigned to the (111), (200), (220) and (311) planes of the Pt face-centred cubic (fcc) crystals (inset in Fig. 3a). A HR-TEM image shown in Fig. 3b displays typical nanodendrites. The inset image indicates a lattice spacing distance of 0.22 nm for one branch of PtPd nanodendrites, which is slightly smaller than 0.23 nm of the {111} lattice spacing of the bulk Pt. This contraction of lattice caused by the addition of Pd is in line with the reported results in literature [35], which indicates the interactions between Pt and Pd atoms in the formed PtPd NDs.

The fast reduction of Pd and their role as growing seeds on GDL surface indicates a non-negligible influence of the amount of Pd on the formation of the final nanostructures. Some early researches have been carried out by other groups to this synthesis for supported and un-supported catalysts [24, 28, 33]. But, all of them only focus on the pure material research, and none of them has demonstrated the real catalytic performance of these nanostructures in practical fuel cells. In particular, when this synthesis is conducted directly on the large-area GDL surface, the effect of Pd is thus different from that in solution or supported-catalysts. Fig. S3 shows TEM images of PtPd nanostructures with various Pd atomic contents. At a high Pd content of 50 at%, a high supersaturation of Pd atoms greatly lowers the free-energy barrier for heterogeneous nucleation and is responsible for the rapid nucleation rate of Pt with a vanishingly small growth rate [36]. Therefore, the main morphology obtained is spherical PtPd nanoparticle aggregate with an average particle size of ca. 5 nm (Fig. S3a). But, when pure Pd is used, rather than Pd nanoparticles obtained as those reported in literature [31, 33, 34], very large Pd crystal grains are observed (Fig. S3e and f). In one case, this indicates the important effects of the existing of Pt ions with Pd in the formation of nanoparticles on the GDL surface, as that with 50 at% Pd. On

10

the other hand, it suggests different crystal growth mechanisms on the large-area GDL as compared with those in solution or on supports. With the decrease of the Pd content, the nucleation sites provided are reduced, and accordingly, short nanodendrites (Fig. S3b) are formed through the reported particle attachment growth process [28]. Decreasing the Pd content to 10 at%, a high yield of nanodendrites is obtained. The branch shows a length of ca. 5–10 nm (Fig. S3c). With a further decrease in Pd, PtPd nanodendrites with longer and dense branches are obtained (i.e. Fig. 3 at 5 at%). At 2.5 at% Pd, the branch length increases to 10–20 nm (Fig. S3d). Therefore, in the presence of a high Pd content nanoparticles are inclined to form, and nanodendrites are achieved when the Pd content decreases.

To further understand the crystal structure of the as-prepared PtPd nanostructures, XRD analysis was performed to the plain GDL 35BC, GDEs of Pt, Pd and PtPd 5 at% (Fig. S4). PtPd 5 at% NDs show the characteristic peaks locating between single Pt (JCPDS-04-0802 Pt) and Pd (JCPDS-46-1043 Pd) [37, 38], indicating the formation of the solid-solution PtPd alloy again, as supported by the HRTEM results (Fig. 3b). The much stronger intensity of the Pd peaks also confirms the very large crystal grains formed (Fig. S3e and f). XPS analysis was conducted to identify near-surface species involved in PtPd heterostructures (Fig. S5). It can be seen that, with the increase of Pd, the intensity of Pd 3d peaks becomes stronger while that of the Pt 4d peaks becomes weaker, and all peaks shift more positively compared with the monometallic Pt (4d3/2 at 331.6 eV) and Pd (3d5/2 and 3d3/2 at 335.2 and 340.5 eV, respectively), suggesting the PtPd interactions [39] change the atomic structure thus contributing to the enhanced activity in PtPd bimetallic hybrids [31].

11

In order to understand the influence of Pd content on the catalytic performance of PtPd nanostructures in real fuel cell conditions, PtPd GDEs fabricated with different Pd contents were directly used as cathodes and tested in 16 cm^2 hydrogen-air PEFCs. Cathode CVs were recorded in-situ in single cells to measure the electrochemical active specific area (ECSA) of catalysts within electrodes. From CVs in Fig. 4, normalized by the metal loading in precursors (checked by TGA shown in Fig. S6), ECSAs for PtPd GDEs with Pd atomic percentages of 50, 25, 10, 5, 2.5 and 0.5, as well as PtNW GDE are 0.49, 7.21, 11.59, 22.40, 18.76, 18.15 and 14.70 m^2 g^{-1}, respectively. The smallest ECSA value of PtPd 50 at% GDE can be ascribed to the nanoparticle aggregates formed on the GDL surface (Fig. S3a). This aggregation reduces contribution of catalysts to the three-phase boundary (TPB) in the electrodes and leads to a low catalyst utilisation ratio in fuel cell electrode [40]. Larger ECSA is obtained as aggregates reduce with a decreased Pd content. When the composition of Pd arrives at 5 at%, a larger ECSA is achieved as expected due to the more regular PtPd NDs achieved. The ECSA of PtPd 2.5 and 0.5 at% GDEs are slightly lower, which can be ascribed to the longer and denser nanodendrite branches (Fig. S3d) and their relative non-uniform distribution on GDLs (Fig. 2a and b). With a similar morphology, the larger ECSA of PtPdND GDEs at the low Pd content than that of PtNW GDE indicates that PtPdND GDE is more electrochemically accessible due to their better distribution on the GDL surface. However, the anisotropic morphology still results in a much lower ECSA for the PtPd ND GDE as compared to the commercial Pt/C nanoparticle catalysts (30.91 m^2 g^{-1}), which is in line with those reported in literature [10,29].

Fig. 5 shows polarization curves and their power densities at 0.6 V of the MEAs with the as-prepared PtPd GDEs, as well as PtNW and Pt/C GDEs. The comparison is conducted at 0.6 V because this is the common voltage used in practical operational conditions of PEFCs. Although a much larger ECSA is observed for Pt/C nanoparticles, the power performance obtained is much lower, and the power density at 0.6 V is only 0.55 W cm^{-2}, while PtNW GDE exhibits a higher value of 0.64 W cm^{-2}. Regarding PtPd GDEs, at a high Pd amount, e.g. 50%, the lower catalyst utilisation ratio from the aggregated nanoparticles finally results in a poor electrode performance. With decrease of the Pd content, a better performance is obtained, reaching the maximum value at 5 at%. At this optimal Pd content, the uniform distribution of NDs enables a more porous catalyst layer, which facilitates oxygen diffusion to the catalyst surface to achieve a reduced mass transfer loss and a higher catalyst utilization ratio, thus a better catalytic performance is expected. Further decrease of the Pd content leads to PtPd NDs with longer and dense branches, as well as the relative non-uniform distribution on GDL surface (Fig. 2 and S3), finally resulting in a lower catalyst utilization ratio and thus a decline of the electrode performance. The power performance of PtPdND GDE with 5 at% Pd exhibits the highest power density of 0.73 W cm^{-2} at 0.6 V, better than those of both PtNP/C and PtNW GDEs, demonstrating the advantages from both the 1D morphology over the 0D nanoparticles and the PtPd hybriding over pure Pt nanowires.

To further understand the effect of the behaviour of PtPd nanostructures on power performance, EIS measurements were conducted at three current densities for PtPd GDEs with different compositions as well as to the Pt/C and PtNW GDEs (Fig. 6). At a low current density of 0.05 A cm^{-2}, the impedance represented by the diameter of

the semi-circle is mainly contributed by charge transfer resistance, indicating ORR catalytic kinetic performance. Fig. 6a shows the largest impedance with the PtPdND GDE with 50 at% Pd. The smallest semicircle is observed for the PtPd GDE with 5 at% Pd, indicating the lowest charge transfer resistance and thus the best ORR catalytic kinetic performance. However, all PtPd GDEs with medium and low Pd contents together with Pt/C and PtNW GDEs show similar impedances, implying a close ORR catalytic kinetic performance for all of them. This is slightly different from those reported higher catalytic activities from the enhanced effect of PtPd over Pt by the measurement conducted in liquid electrolytes [20]. Although the clear mechanism is still not clear now, it can possibly ascribed to the much complex test environment in practical fuel cells compared with that in the liquid electrolyte. Here, besides the intrinsic catalytic activities, the catalyst behaviour and their surrounding environment in electrode together determine the final performance in fuel cells. With the increase of the current density (Fig. 6b and c), the 2nd semicircle appears on EIS which mainly represents mass transfer resistance within electrodes. PtPdND GDE with 5 at% Pd still shows the smallest charge and mass transfer resistance, while the GDEs with Pt/C nanoparticles and PtPd GDE 50 at% exhibit very large resistances due to their dense electrode structure. These EIS measurement results demonstrate the much reduced mass transfer loss in the PtNW GDE as compared with those from both PtPd and Pt nanoparticles, and a further improvement can also be achieved by introducing a small amount of Pd to optimise their distribution on GDL surface.

Besides catalytic activities, a high stability is also usually reported for PtPd hybrid structures over Pt [41], which is based on the enhanced effect of Pd and Pt preventing the dissolution of catalysts during the potential cycling. To check the effect of

14

introducing Pd to the as-prepared PtPd NDs on the GDE performance in fuel cells, an accelerated degradation test (ADT) was carried out by 3000 potential sweeping cycles in the single cell at room temperature. Cathode CVs after the ADT test are displayed with the initial curves and compared with those of PtNWs and Pt/C nanoparticles in Fig. 7a. After the ADT, all GDEs exhibit a big decline of their ECSAs, and a lower ratio is observed to the PtPdND GDE as compared with PtNW one, which agrees well with those reported in literature [37, 38], but the one from Pt/C shows the least drop. The remaining values of PtNW, PtPdND and Pt/C GDEs are 5.55, 11.96 and 21.25 m^2 g^{-1}, corresponding to 62.2%, 46.6% and 31.2% loss of their initial ECSAs, respectively (Fig. 7c). Fig. 7b shows polarization curves for all GDEs after the ADT. It can be seen that the PtPdND GDE still exhibits a higher power performance than the PtNW GDE at 0.6 V, and the Pt/C GDE shows a very low performance, corresponding to degradation ratios of 19.9%, 12.7% and 27.5% (Fig. 7d), respectively. At the high voltage region (>0.7V), PtNW GDE presents a higher power performance, indicating a better kinetic activity than PtPdND GDE, which can be explained by the higher mass activity remained after the ADT [11,40]. The larger ratio of ECSA loss than the lower degradation percentage of power performance indicates the increase in the specific area activity of catalysts [42], and the result shown here indicates this improvement becomes larger with the increase of the aspect ratio from nanoparticles, NDs to NWs. Although the detailed mechanisms are still not clear at the moment [1], this phenomenon further demonstrates advantages of 1D nanostructured catalysts for PEFC applications.

4. Conclusions

In summary, we have demonstrated a catalyst electrode from PtPd nanodendrites in-situ grown on large-area gas diffusion layer carbon paper surface by a facile wet chemical procedure. The experimental results show that the content of Pd greatly influences the final morphology and distribution of PtPd nanostructures on GDL surfaces, which together determines the final power performance in PEFC applications. The introducing of an optimal amount of Pd, i.e. 5 at% to Pt nanowire growth leads to more uniform distributed PtPd nanodendrites on the GDL surface, reducing the mass transfer resistance within the electrode to achieve a high power performance. Besides, PtPd NDs exhibit a higher power performance over Pt NWs even after the durability test in PEFCs, showing a lower loss of ECSA but a higher degradation percentage of power performance. Due to an analogous catalyst electrode could be formed based on other hybrid anisotropic nanostructures, the results here point to new electrode preparation strategies that leverage both the catalyst intrinsic activity and the electrode structure for high performance PEFCs.

Acknowledgements

Supporting Information

Supporting information includes additional information on the UV-Vis spectra, EDX analysis results, SEM images of Pd grown on GDL, TGA curves and a comparison of polarization curves of PtPd GDE fabricated by two growing procedures.

References

[1]   C. Koenigsmann, S.S. Wong, Energ Environ Sci 4 (2011) 1161-1176.

[2]   G. Zhang, S. Sun, M. Cai, Y. Zhang, R. Li, X. Sun, Sci Rep 3 (2013) 1526.

[3]   S. Sun, G. Zhang, D. Geng, Y. Chen, R. Li, M. Cai, X. Sun, Angewandte Chemie Int Ed 50 (2011) 422-426.

[4]   S.M. Alia, G. Zhang, D. Kisailus, D. Li, S. Gu, K. Jensen, Y. Yan, Adv Funct Mater 20 (2010) 3742-3746.

[5]   B.Y. Xia, W.T. Ng, H.B. Wu, X. Wang, X.W. Lou, Angew Chem Int Ed 51 (2012) 7213–7216.

[6]   L.Y. Ruan, E.B. Zhu, Y. Chen, Z.Y. Lin, X.Q. Huang, X.F. Duan, Y. Huang, Angew Chem Int Edit 52 (2013) 12577-12581.

[7]   S. Du, Int J Low-Carbon Tech 7 (2012) 44-54.

[8]   S. Sun, G. Zhang, D. Geng, Y. Chen, M.N. Banis, R. Li, M. Cai, X. Sun, Chem –Eur J 16 (2010) 829-835.

[9]   S.F. Du, J. Power Sources 195 (2010) 289-292.

[10]   S.F. Du, K.J. Lin, S.K. Malladi, Y.X. Lu, S.H. Sun, Q. Xu, R. Steinberger-Wilckens, H.S. Dong, Sci Rep 4 (2014) 6439.

[11]   Y.X. Lu, S.F. Du, R. Steinberger-Wilckens, Appl Catal B-Environ 164 (2015) 389-395.

[12]   X.Y. Yao, K.H. Su, S. Sui, L.W. Mao, A. He, J.L. Zhang, S.F. Du, Int J Hydrogen Energ 38 (2013) 12374-12378.

[13]   L. Su, S. Shrestha, Z. Zhang, W. Mustain, Y. Lei, J Mater Chem A 1 (2013) 12293-12301.

[14] I.E.L. Stephens, A.S. Bondarenko, U. Gronbjerg, J. Rossmeisl, I. Chorkendorff, Energ Environ Sci 5 (2012) 6744-6762.

[15] J. Greeley, I.E.L. Stephens, A.S. Bondarenko, T.P. Johansson, H.A. Hansen, T.F. Jaramillo, J. Rossmeisl, I. Chorkendorff, J.K. Norskov, Nat Chem 1 (2009) 552-556.

[16] Y.H. Bing, H.S. Liu, L. Zhang, D. Ghosh, J.J. Zhang, Chem Soc Rev 39 (2010) 2184-2202.

[17] W.T. Yu, M.D. Porosoff, J.G.G. Chen, Chem Rev 112 (2012) 5780-5817.

[18] C. Koenigsmann, S.S. Wong, ACS Catal 3 (2013) 2031-2040.

[19] Y.J. Deng, N. Tian, Z.Y. Zhou, R. Huang, Z.L. Liu, J. Xiao, S.-G. Sun, Chem Sci 3 (2012) 1157-1161.

[20] H. Zhang, M.S. Jin, Y.N. Xia, Chem Soc Rev 41 (2012) 8035-8049.

[21] Z. Zhu, Y. Zhai, C. Zhu, Z. Wang, S. Dong, Electrochem Commun 36 (2013) 22-25.

[22] S.M. Alia, K.O. Jensen, B.S. Pivovar, Y. Yan, ACS Catal 2 (2012) 858-863.

[23] B. Lim, M. Jiang, T. Yu, P.C. Camargo, Y. Xia, Nano Res 3 (2010) 69-80.

[24] S. Ghosh, S. Mondal, C. Retna Raj, J Mater Chem A 2 (2014) 2233-2239.

[25] Y.Z. Lu, Y.Y. Jiang, W. Chen, Nano Energy 2 (2013) 836-844.

[26] C. Zhu, S. Guo, S. Dong, Adv Mater 24 (2012) 2326-2331.

[27] S.J. Guo, S.J. Dong, E.K. Wang, Chem Commun 46 (2010) 1869-1871.

[28] J.-J. Lv, J.-N. Zheng, S.-S. Li, L.-L. Chen, A.-J. Wang, J.-J. Feng, J Mater Chem A 2 (2014) 4384-4390.

[29] S.H. Sun, F. Jaouen, J.P. Dodelet, Adv Mater 20 (2008) 3900-3904.

[30] S.H. Sun, D.Q. Yang, D. Villers, G.X. Zhang, E. Sacher, J.P. Dodelet, Adv Mater 20 (2008) 571-574.

[31] S. Du, Y. Lu, R. Steinberger-Wilckens, Carbon 79 (2014) 346-353.

[32] X. Chen, Z. Cai, X. Chen, M. Oyama, J Mater Chem A 2 (2014) 315.

[33] L. Wang, Y. Yamauchi, Chem-Asian J 5 (2010) 2493-2498.

[34] S.J. Guo, S.J. Dong, E.K. Wang, ACS Nano 4 (2010) 547-555.

[35] Y. Kim, Y. Noh, E.J. Lim, S. Lee, S.M. Choi, W.B. Kim, J Mater Chem A 2 (2014) 6976-6986.

[36] A. Cacciuto, S. Auer, D. Frenkel, Nature 428 (2004) 404-406.

[37] X. Yang, Q.D. Yang, J. Xu, C.S. Lee, J Mater Chem 22 (2012) 8057-8062.

[38] Y.C. Tseng, H.S. Chen, C.W. Liu, T.H. Yeh, K.W. Wang, J Mater Chem A 2 (2014) 4270-4275.

[39] C.Z. Zhu, S.J. Guo, S.J. Dong, Adv Mater 24 (2012) 2326-2331.

[40] H.A. Gasteiger, S.S. Kocha, B. Sompalli, F.T. Wagner, Appl Catal B-Environ 56 (2005) 9-35.

[41] L.X. Ding, C.L. Liang, H. Xu, A.L. Wang, Y.X. Tong, G.R. Li, Adv Mater Interfaces (2014) 1400005.

[42] P. Hernandez-Fernandez, F. Masini, D.N. McCarthy, C.E. Strebel, D. Friebel, D. Deiana, P. Malacrida, A. Nierhoff, A. Bodin, A.M. Wise, J.H. Nielsen, T.W. Hansen, A. Nilsson, I.E.L. Stephens, I. Chorkendorff, Nat Chem 6 (2014) 732-738.

Figure captions:

Fig. 1 Illustration of fuel cell setup.

Fig. 2 SEM images of (a, b) PtNW GDE and (c, d) PtPd GDE with 5 at% Pd. (a, c) and (b, d) show the edge and center area of the two GDE pieces, respectively.

Fig. 3 TEM images of PtPd nanostructures with 5 at% Pd in-situ grown on GDL surface. Insets in (a) and (b) show the SAED pattern and HR-TEM image of one branch, respectively.

Fig. 4 Cathode CVs for GDEs from Pt/C, PtNWs and PtPdNDs with different compositions.

Fig. 5 (a) Polarization curves and (b) the trend of the power density at 0.6 V for PtPd GDEs with different Pd contents and PtNW and Pt/C GDEs.

Fig. 6 EIS measured at (a) 0.05, (b) 0.5 and (c) 1.0 A cm^{-2} for PtPdND GDEs with various Pd contents, PtNW and Pt/C GDEs.

Fig. 7 (a) CVs, (b) polarization curves, (c) ECSAs and (d) power densities at 0.6 V for GDEs from PtPdNDs with 5 at% Pd, PtNWs and Pt/C nanoparticles before and after the ADT test.
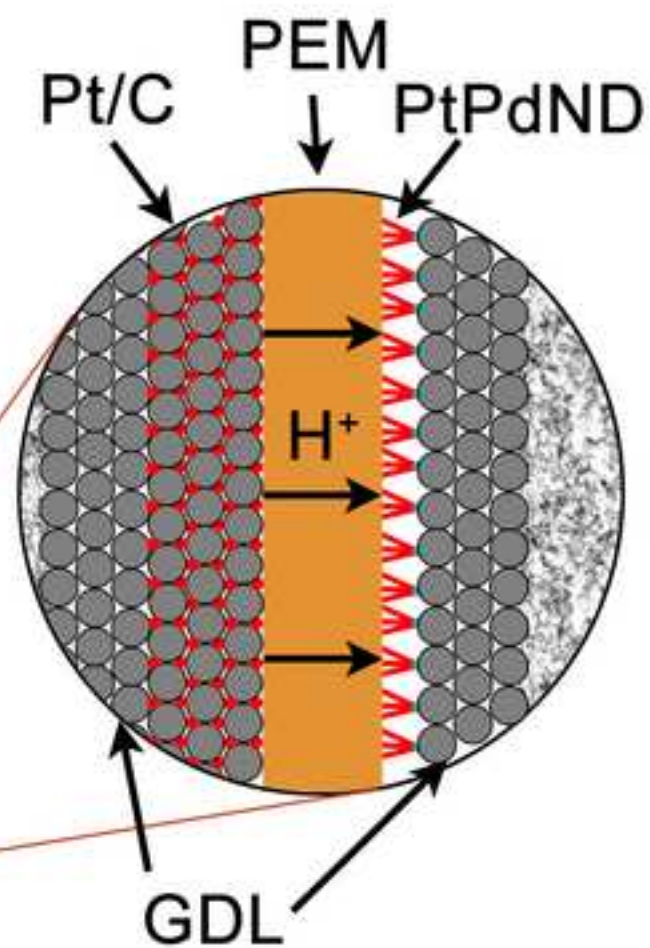
Figure 1

Figure 2
Click here to download high resolution image

a) (200) (111) (220) (311) 50 nm

b) 0.22 nm 0.22 nm 5 nm
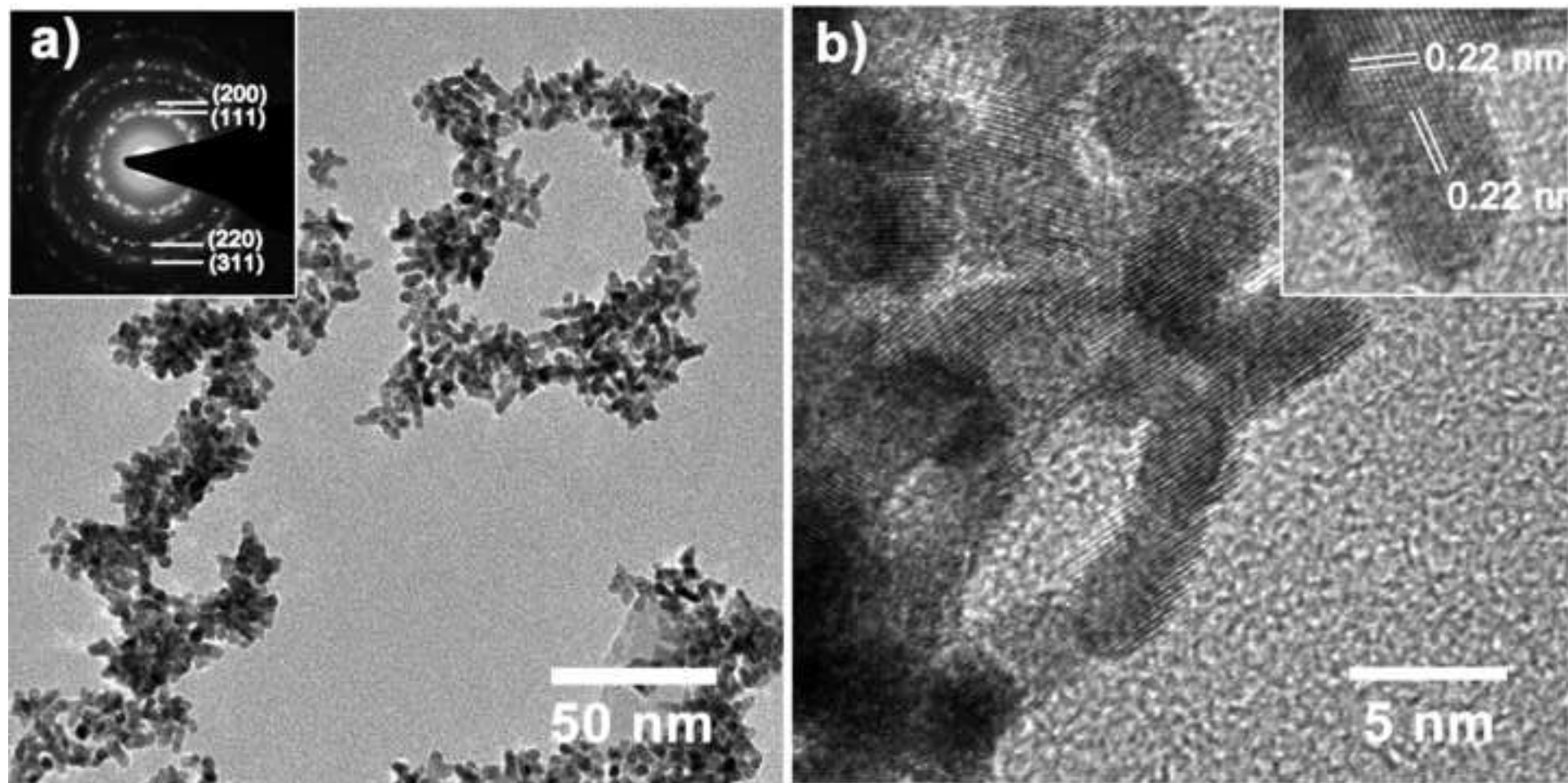
Figure 4
Click here to download high resolution image
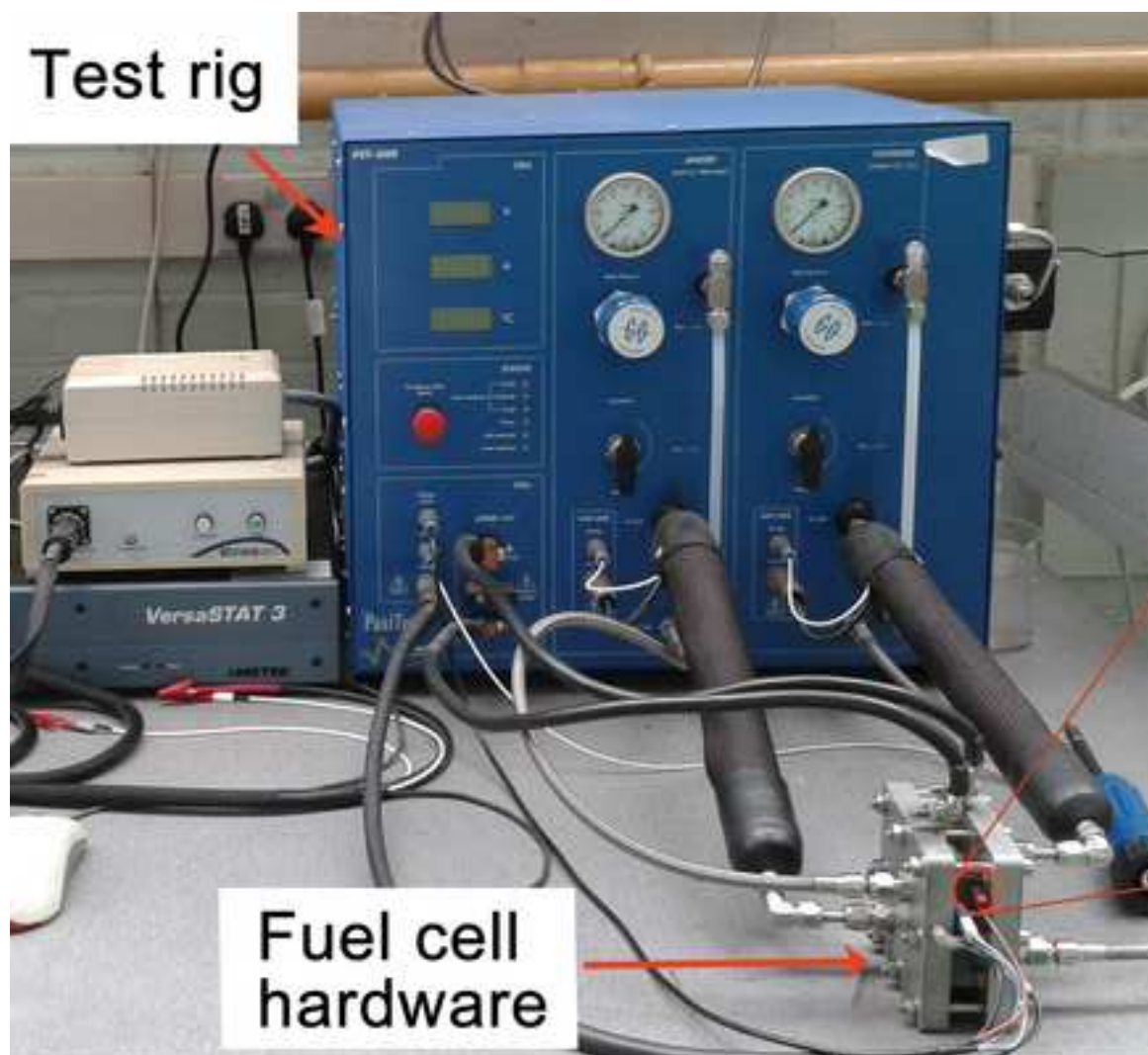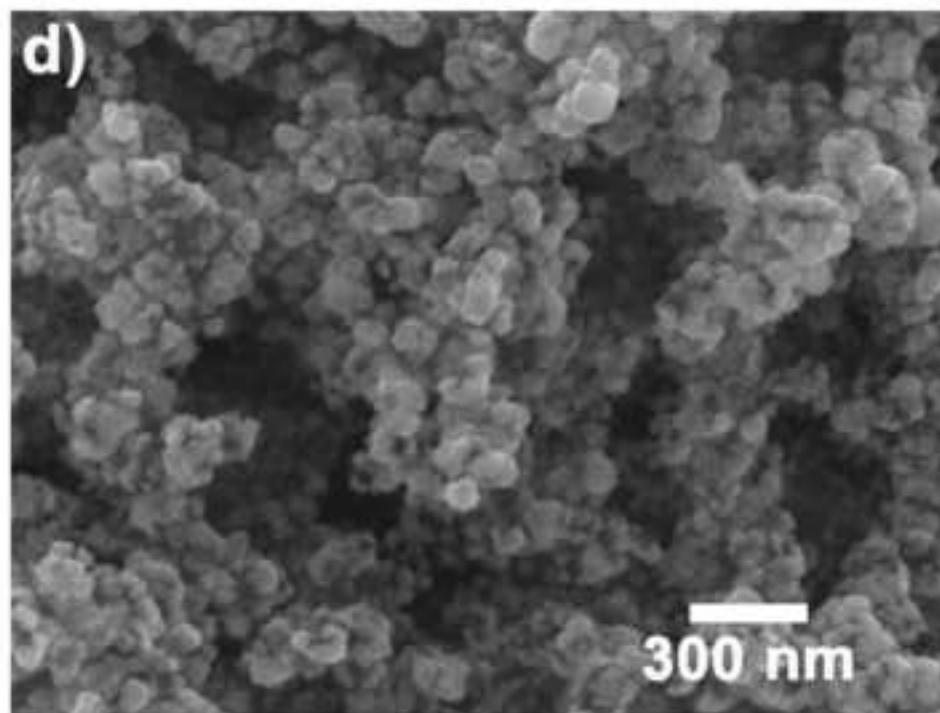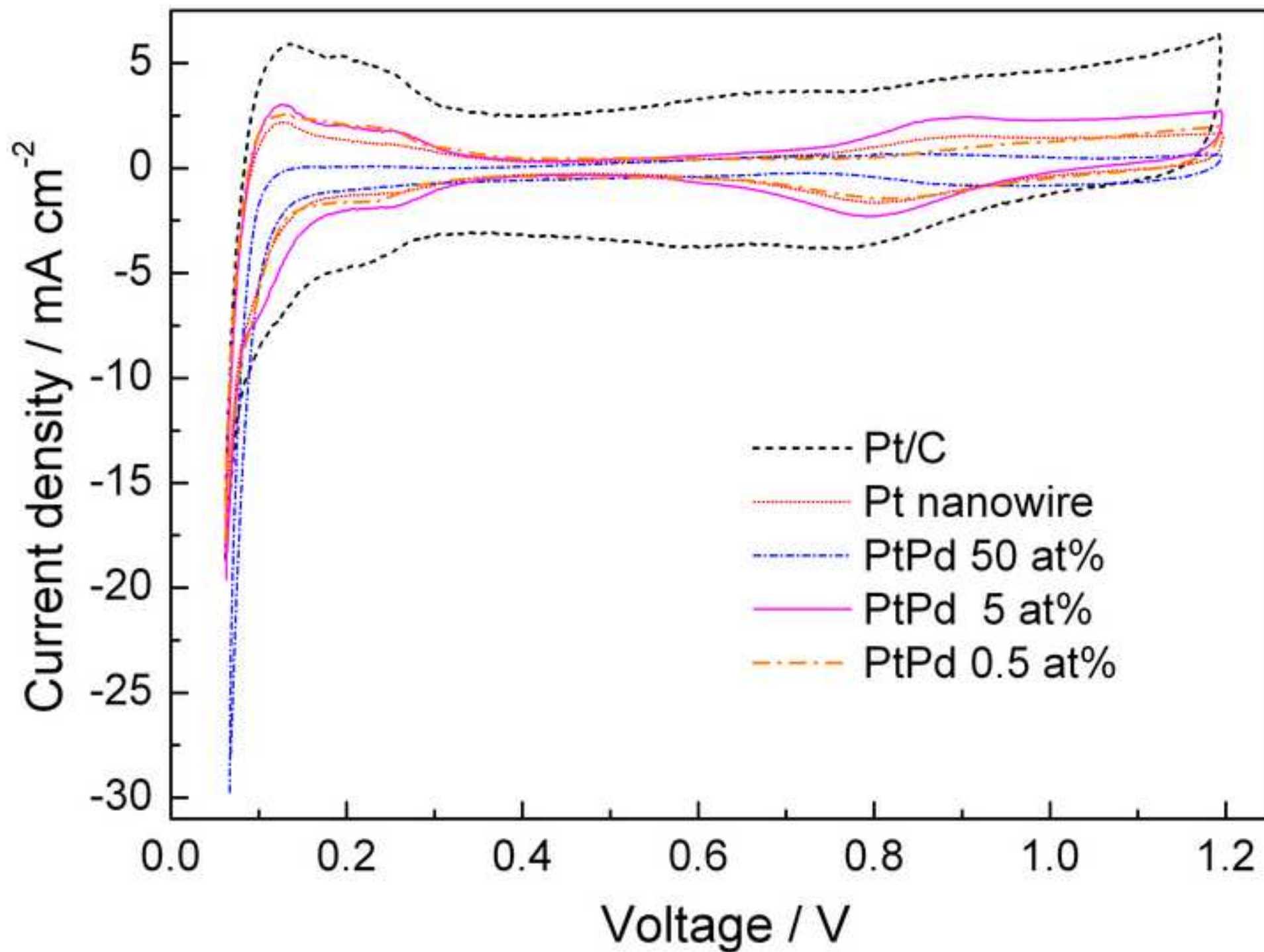
Figure 5
Click here to download high resolution image
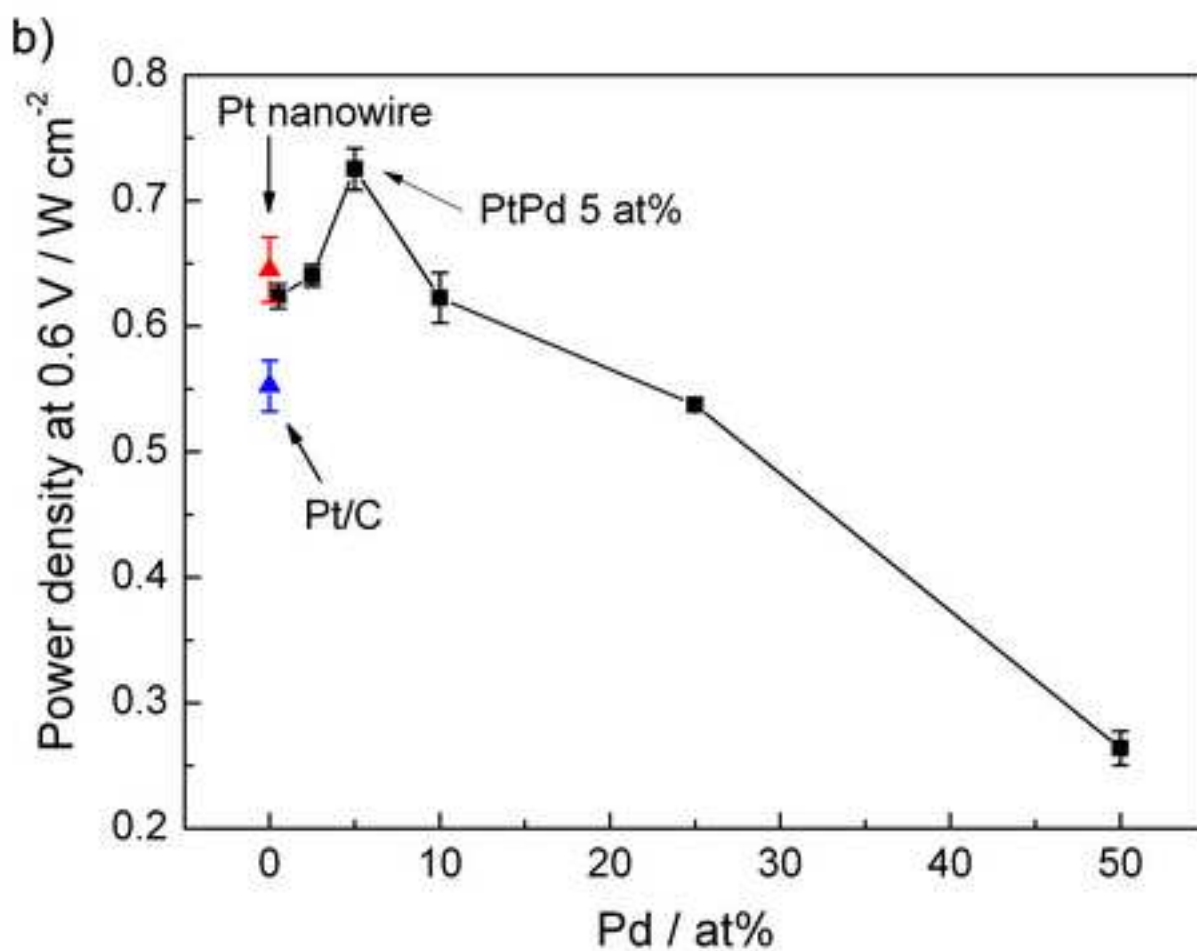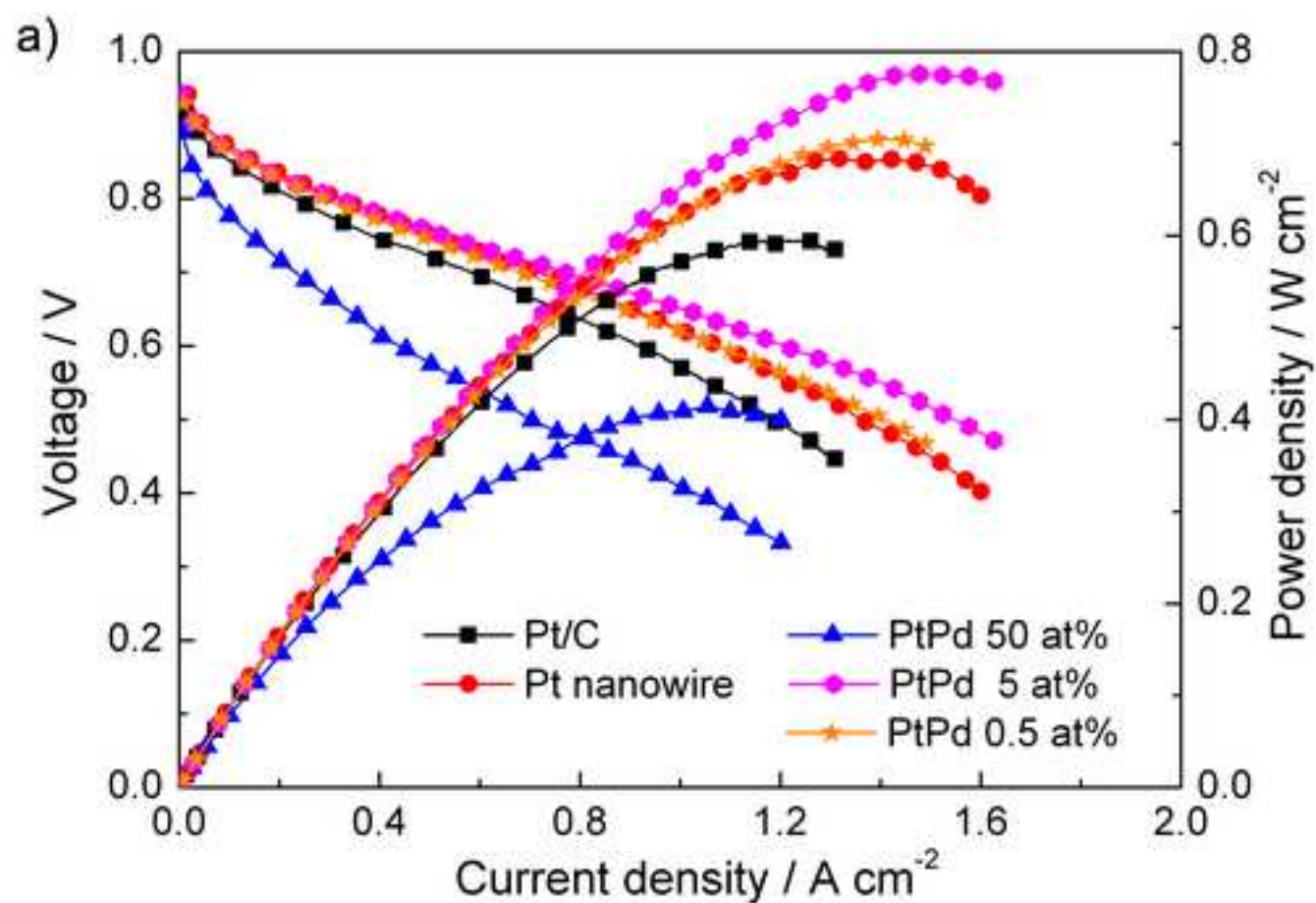
Figure 6
[Click here to download high resolution image](#)
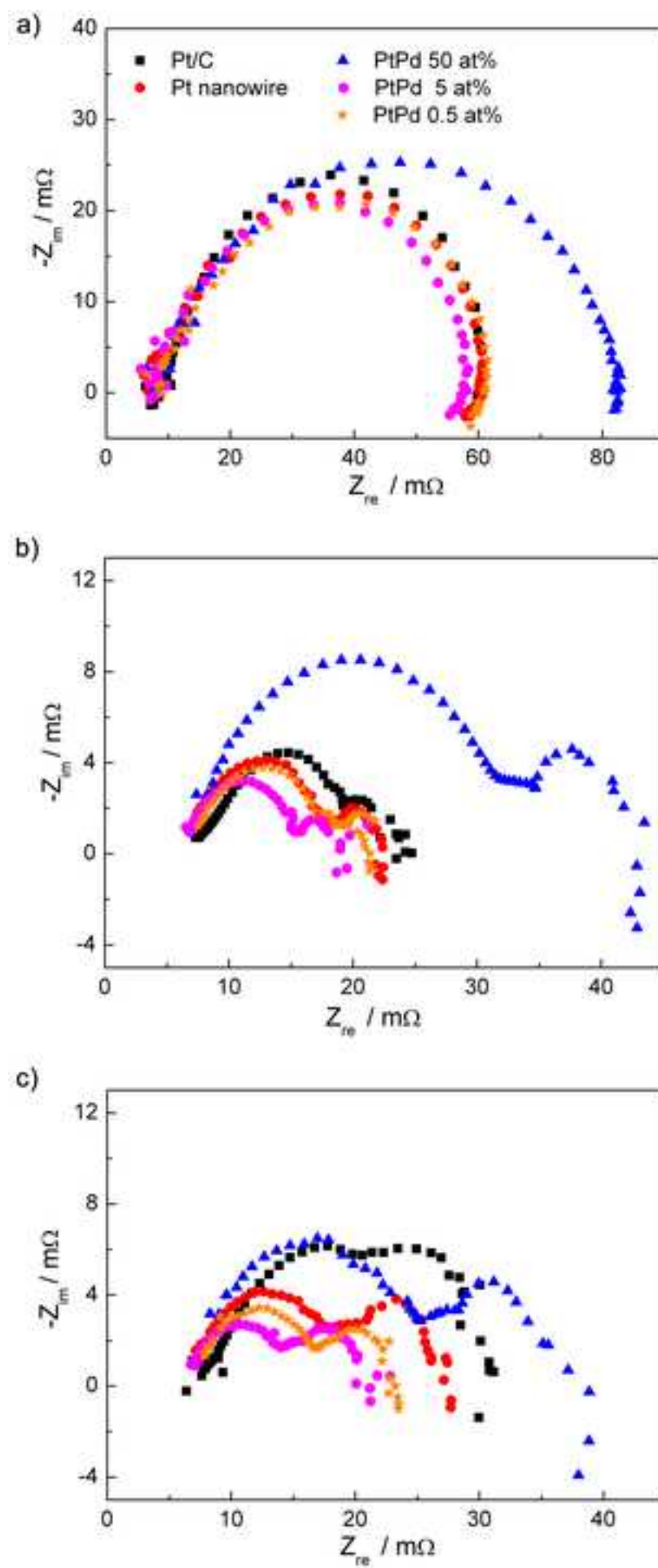
Figure 7
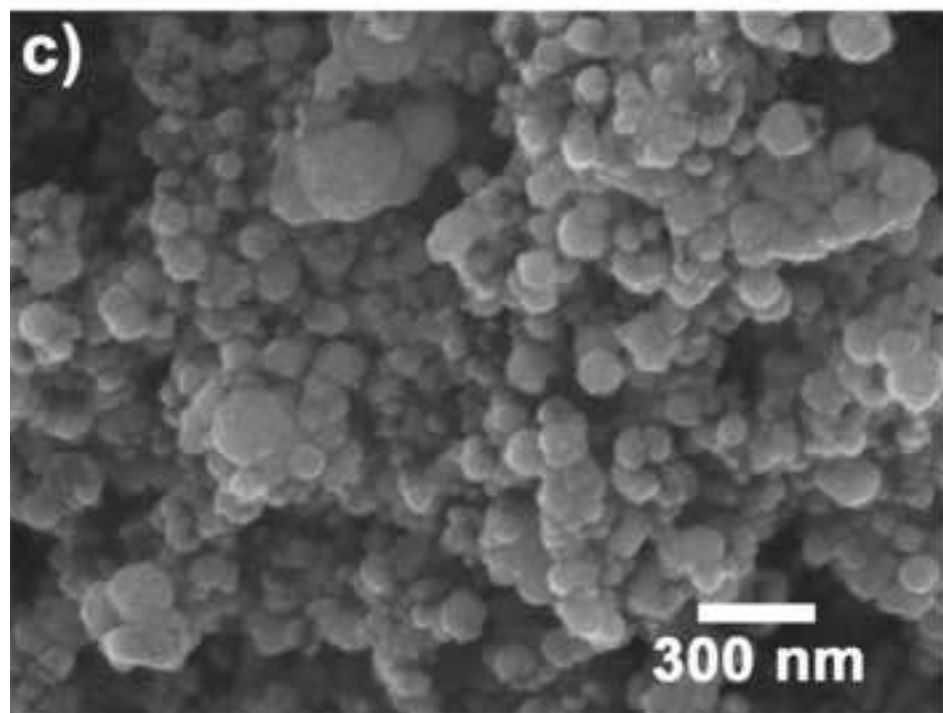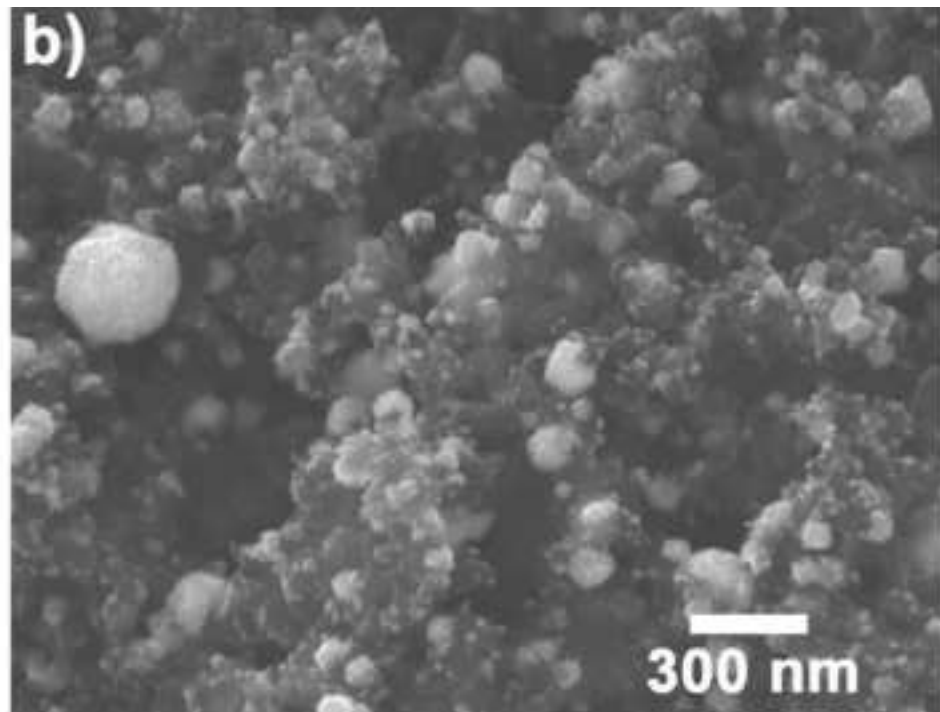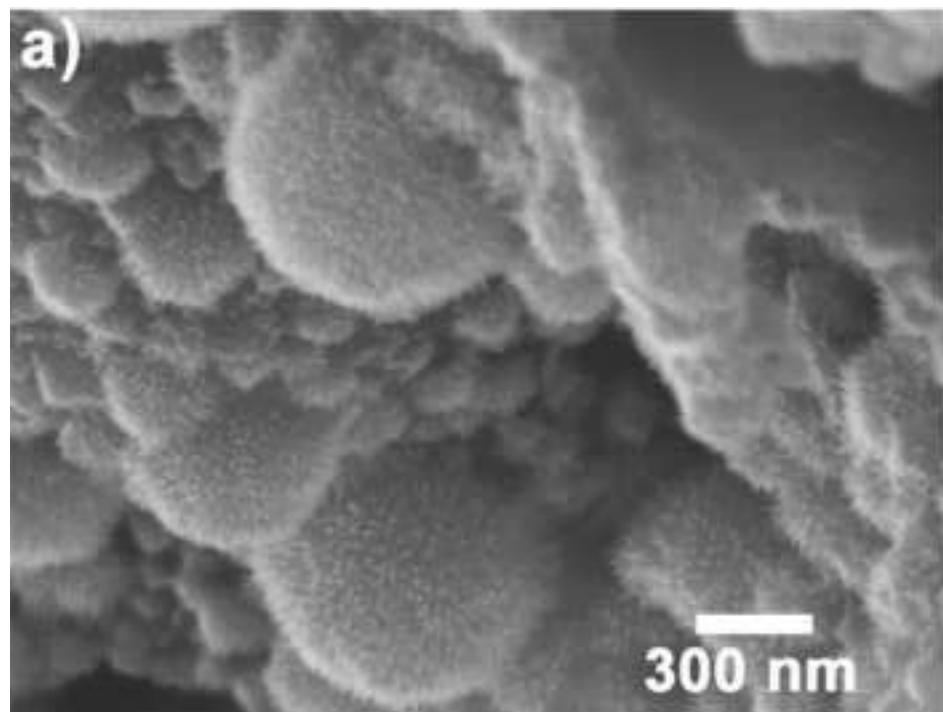[Click here to download high resolution image](#)

PtPd
nanodendrites
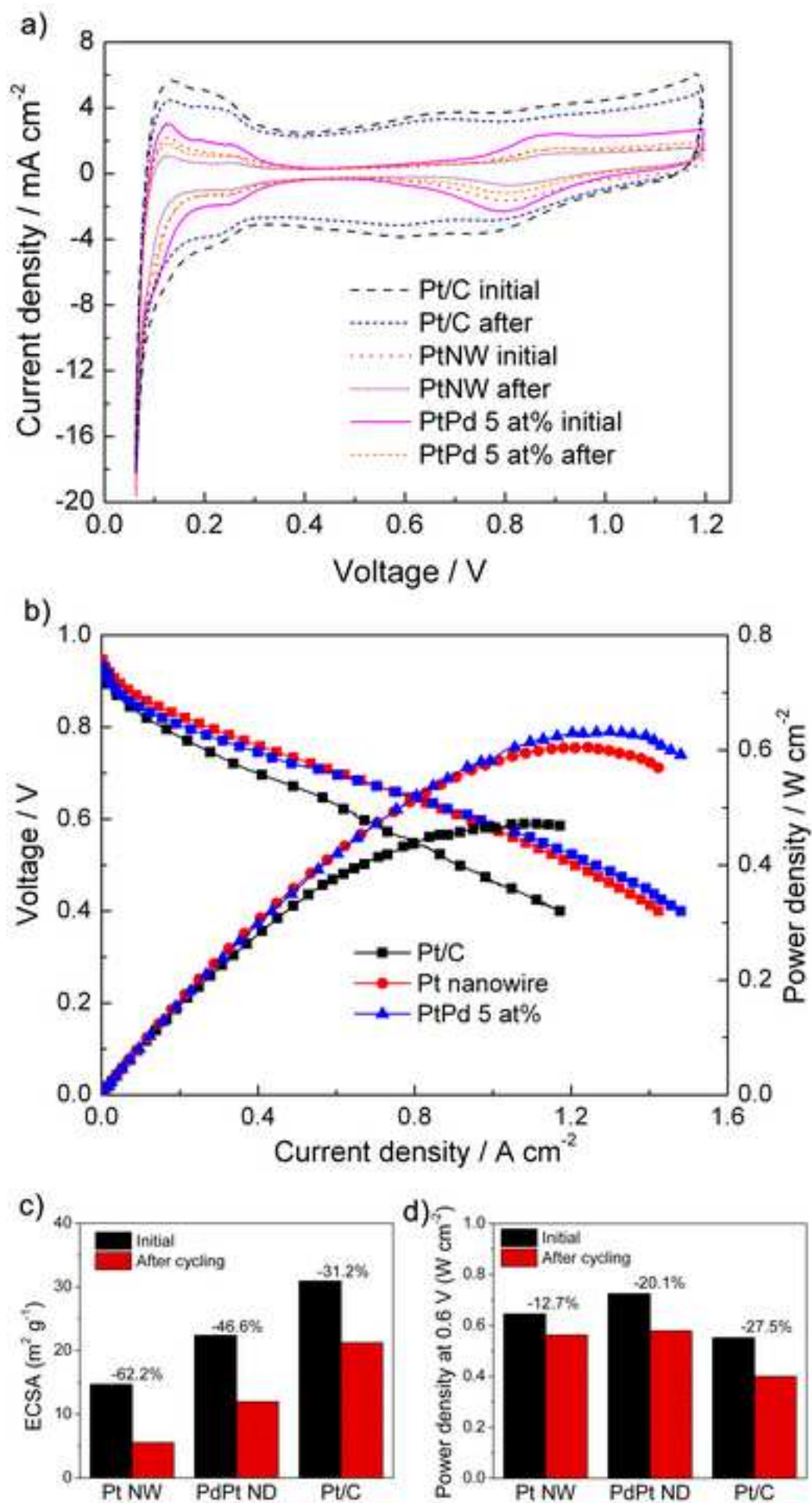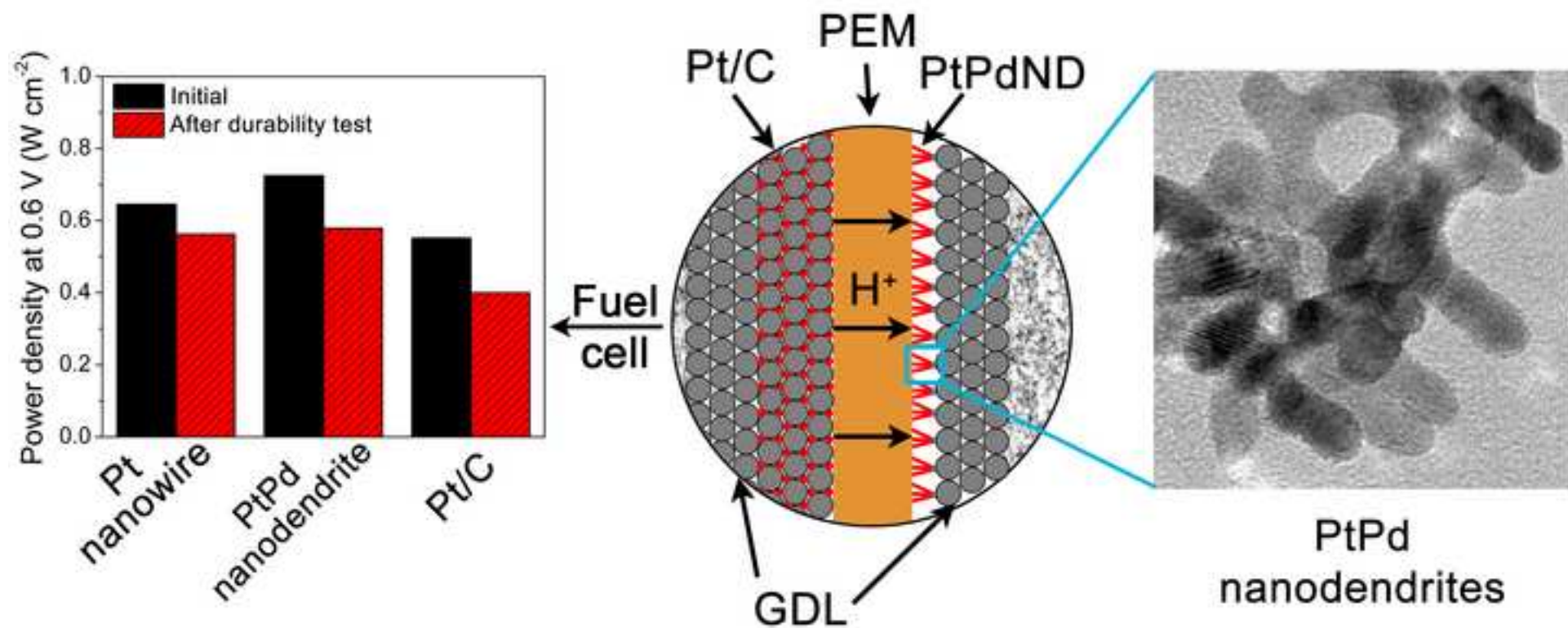
Highlights

- Direct catalyst electrodes from PtPd nanodendrites for PEFC applications
- In-situ growing PtPd nanodendrites on 16 cm^2 GDL carbon paper surface
- Direct evidences for crystal growth mechanisms of PtPd nanodendrites
- Pd affects both morphology and distribution of PtPd nanostructures on GDL surface
- Thin catalyst layer with PtPd nanodendrites reduces mass transfer losses

Supplementary Material

Three-dimensional catalyst electrodes based on PtPd nanodendrites for oxygen reduction reaction in PEFC applications

Yaxiang Lu, Shangfeng Du[*], Robert Steinberger-Wilckens

School of Chemical Engineering, University of Birmingham, Edgbaston, Birmingham B15 2TT, UK

To whom correspondence should be addressed to:

*SF Du: E-mail: s.du@bham.ac.uk, Tel: +44-121-4158696

1

Abstract

PtPd bimetallic nanodendrites (NDs), with enhanced activities from PtPd over element Pt and unique anisotropic morphology, show potential as catalysts in fuel cell applications. However, the research has been limited to pure materials, and constructing a practical fuel cell catalyst electrode from PtPd NDs still remains as a challenge. In this paper, we demonstrated, for the first time, catalyst electrodes from PtPd NDs for polymer electrolyte fuel cell (PEFC) applications. PtPd NDs are in-situ grown on large-area carbon paper gas diffusion layers (GDLs) and directly employed as cathodes in H_2/air PEFCs. The thin catalyst layer with PtPd nanodendrites significantly reduces mass transfer resistance and a higher power performance is achieved than those based on pure Pt nanowires and Pt/C nanoparticle electrocatalysts. The crystal growth mechanisms of this advanced nanostructure on large-area support are also detailed based on the time-dependent experiments and Pd content.

1. Introduction

Due to unique properties, one-dimensional (1D) nanostructures such as nanodendrites (NDs), nanowires (NWs) and nanotubes (NTs) have been widely studied for their enhanced catalytic activities toward fuel cell reactions [1-4]. Compared with associated zero-dimensional (0D) nanoparticles (NPs), 1D nanostructures have more enhanced reaction kinetics on catalyst surface and are less vulnerable to dissolution and aggregation, which can potentially improve their catalytic activity and durability [5-7]. Benefiting from these advantages, three-dimensional (3D) nanostructures based on 1D Pt nanowire arrays have been fabricated by bottom-up design and demonstrated as effective catalyst electrodes to address some challenges faced by the conventional fuel cell electrodes with Pt-based NPs [8, 9]. These 3D catalyst electrodes have been confirmed with high performance in real fuel cells owing to a high catalyst utilisation ratio resulted from a significantly reduced mass transfer resistance induced by the thin and porous catalyst layer, as well as unique catalytic properties of single-crystal Pt NWs [10-12].

Although Pt is still the best electrocatalyst for the oxygen reduction reaction (ORR) in cathodes for polymer electrolyte fuel cells (PEFCs), the relative high cost, and in particular the poor stability are still the major limits for the successful commercialization of this technology [13, 14]. In order to improve the stability and reduce the loading of precious Pt while not compromising the activity, one promising strategy is to introduce other element into Pt to form alloy or hybrid catalysts [15, 16]. It is generally accepted that the incorporation of a second metal component can offer desired interactions with Pt to tune both electronic and surface effects, triggering enhanced effects to improve physical and chemical properties [17, 18]. Sitting in the

same periodic group as Pt and possessing a similar lattice space, Pd has been confirmed as a promising candidate [19, 20]. 1D Pt-Pd bimetallic electrocatalysts with various structures such as alloy [21], core-shell [22] and heterostructure as well as different morphologies like nanodendrites [23, 24], nanowires [21], nanotubes [22], nanorods [25] etc. have been reported. The advantages of the bimetallic feature and 1D anisotropic properties lead to an improved catalysis process [26-28], resulting in a long-term stability and also superior activity toward ORR. Some references also indicated that the existence of Pd played a significant role on the morphology of Pt-Pd bimetallic nanostructures [28]. For example, Xia's group [23] reported that in the presence of Pd, open branched PtPd dendrites were formed, otherwise only foam-like Pt aggregates were obtained. However, these investigations all focus only on the pure material research, and the real applications of 1D Pt-Pd bimetallic catalysts in practical fuel cells still remains as a challenge.

Inspired by the 3D Pt-nanowire (PtNW) catalyst electrodes and considering the enhanced activity between Pd and Pt, in this work, direct catalyst electrodes with PtPd bimetallic NDs in-situ grown on 16 cm^2 gas diffusion layers (GDLs) are demonstrated. The crystal growth mechanism and influence of Pd on the PtPd nanostructure are studied based on the time-dependent in-situ growing process and the Pd content. The fabricated gas diffusion electrodes (GDEs) with 3D PtPd bimetallic nanostructures are directly tested as cathodes in H_2/air PEFCs. The polarization curves, electrochemical impedance spectra (EIS), cathode cyclic voltammograms (CVs) and accelerated degradation test (ADT) are performed in-situ in PEFCs to investigate the enhanced power performance and durability of PdPtND GDEs.

4

2. Experimental Section

2.1 Chemicals and materials

Hexachloroplatinic acid hexahydrate ($H_2PtCl_6 \cdot 6H_2O$, $\geq 37.50\%$ Pt basis) and palladium(II) chloride ($PdCl_2$, anhydrous, 60% Pd basis) from Sigma-Aldrich UK were used as metal precursors. Formic acid (CH_2O_2, 98+%) and isopropanol (IPA) (C_3H_8O, >99.5%) were obtained from Fisher Scientific UK. DuPont Nafion$^®$ 212 membrane, Nafion$^®$ solution (D1021, 10 wt%) and SIGRACET$^®$ GDL 35 BC carbon paper were purchased from Ion Power Inc. 20 wt% Pt supported on Vulcan XC-72 was purchased from Fuel Cell Store. All chemicals and materials were used as received without any further purification. The GDL 35 BC carbon paper was used as the direct substrate for PtPd nanostructure growth. Gas diffusion electrodes (GDEs) with Pt/C catalysts at a loading of 0.4 mg_{Pt} cm^{-2} printed on SIGRACET$^®$ GDL 34 BC were obtained from Johnson Matthey Fuel Cells Ltd and used as anodes for fabricating single cells. Ultrapure water (18.2 MΩ cm) from a Millipore water system was used throughout.

2.2 PtPd GDE preparation and physical characterization

Pieces of 4×4 cm^2 standard GDL 35 BC carbon paper was used as the substrate. It consists of a carbon fibre layer at the back and a top micro porous layer (MPL) from carbon spheres with a particle size of 50–100 nm. The GDL has been treated with polytetrafluoroethylene (PTFE) to give super hydrophobic property to prevent the water flooding in fuel cell operation. PtPd nanostructures with various molar ratios were grown on carbon paper <mark>at MPL surface</mark> by a modified wet chemical reduction method from our previous studies [31]. In a typical synthesis, to ensure the total metal loading of 0.4 mg cm^{-2} on a 16 cm^2 carbon paper, a controlled amount of H_2PtCl_6 and

5

PdCl$_2$ solution coupled with 0.53 mL formic acid were added to 10.6 mL water. Then the carbon paper was immersed in the mixed solution at the bottom in a 6 cm glass Petri dish and stored at room temperature for PtPd nanostructure growth. After the colour of the solution changed from yellow to colourless and the growth process was completed, the samples were rinsed using water and IPA, followed by drying at 40 ^{o}C overnight. The as-prepared carbon paper samples with in-situ grown PtPd nanostructures at various Pd atomic percentages of 50, 25, 10, 5, 2.5 and 0.5 were directly used as GDEs at cathode for PEFCs.

The distribution and morphology of PtPd nanostructures in electrodes were characterized by a field emission scanning electron microscope (FE-SEM, JEOL 7000F, operating at 20 kV) and a high-resolution transmission electron microscope (HR-TEM, Philips CM200 FEG). TEM samples were prepared by scraping catalysts from GDE surface and dispersed onto Cu grids. X-ray diffraction (XRD) patterns were recorded with a Siemens D5005 powder X-ray diffractometer operated at 40 kV and 30 mA using Cu Kα (λ= 0.15418 nm) radiation. X-ray photoelectron spectroscopy (XPS) characterization was conducted on an XPS spectrometer (K-Alpha, Thermo Scientific) with a micro-focussed monochromatized Al Kα radiation.

2.3 Membrane electrode assembly (MEA) fabrication

Membrane electrode assemblies (MEAs) with an active area of 16 cm^2 were fabricated using the as-prepared PtPd GDEs as cathodes and the Pt nanoparticle GDEs from Johnson Matthey as anodes. GDEs were first coated with a thin layer of Nafion ionomer at a loading of 0.6 mg cm^{-2}, and then sandwiched at both sides of a 6$\times$6 cm^2 Nafion 212 membrane. After that, the assembly was hot pressed at 125 ^{o}C

under a pressure of 4.9 MPa for 2 min. An illustration of the MEA setup is shown in Fig. 1. For comparison, MEAs with cathodes based on Pt/C (20 wt%) nanoparticle catalysts and pure Pt nanowires at a Pt loading of 0.4 mg_{Pt} cm^{-2} were also fabricated simultaneously.

2.4 Fuel cell tests

The fabricated MEAs were tested in a PEFC test stand (PaxiTech-BioLogic FCT-50S, Fig. 1) with electrochemical impedance spectroscopy (EIS) capabilities. The gasket used in fuel cell testing was PTFE sheet with a thickness of 254 μm at both cathode and anode sides. All tests were conducted at 70 ^{o}C with fully humidified H_2 and air fed at stoichiometry of 1.3/2.4 and backpressure of 2 bars at the anode and cathode, respectively. The MEAs were conditioned by a break-in at 0.6 V for 7 h, and after that polarization curves were recorded at a scan rate of 5 mV s^{-1} from 0.3 V to open circuit voltage (OCV). EIS measurements were performed in the frequency range from 10 kHz to 0.1 Hz with amplitudes of 0.05, 1 and 2 A at current densities of 0.05, 0.5 and 1 A cm^{-2} for 16 cm^2 PEFCs, respectively.

Cathode cyclic voltammograms (CVs) were recorded using an EZstat-Pro system integrated with the test stand. The cell temperature and backpressure were 25 ^{o}C and 0 bar, respectively. The cathode was fed with fully humidified N_2 at 300 mL min^{-1}, and the anode was fed with fully humidified pure H_2 at 120 mL min^{-1} serving as both reference and counter electrodes, also called a dynamic hydrogen electrode (DHE). Then the cathode potential was cycled between 0.05 and 1.2 V versus DHE at 20 mV s^{-1} for 5 cycles, and the fifth cycle was recorded. Accelerated degradation test (ADT)

was undertaken by potential cycling between 0.6 and 1.2 V for 3000 cycles at a scan rate of 50 mV s^{-1}.

3. Results and discussion

The controlled growth of PtPd nanostructures on 16 cm^2 GDLs was realized by reducing $H_2PtCl_6 \cdot 6H_2O$ and $PdCl_2$ with formic acid in aqueous solution at room temperature [29, 30]. The composition of PtPd nanostructures was tuned by the amount of precursors added in the reaction system while keeping the total metal loading at 0.4 mg cm^{-2}. Since the GDL surface consists of only the inert carbon spheres coated with hydrophobic PTFE, only limited rough sites of carbon sphere surface can serve as the main heterogeneous nucleation sites in the reduction. In our previous research it has also demonstrated that on this kind of surface, the edge area of GDL piece is usually easier to be wetted and provides more nucleation sites than the central region in an aqueous solution [11]. In this case, the population of Pt nuclei multiplies at the edge area while fewer are in the center; therefore more catalyst nanostructures are formed and accumulate at the edge of the GDL piece to form large agglomerates. Comparing with the standard reduction potential of $PtCl_6^{2-}$/Pt (0.73 V vs. standard hydrogen electrode (SHE)), the value for Pd^{2+}/Pd couple is more positive (0.92 V vs. SHE), meaning that Pd nuclei can form on the GDL surface much easier than Pt [28]. This relative positive standard reduction potential enables the generated Pd nanoparticles distribute more uniformly on the inert surface, which then act as seeds to induce the co-reduction and further growth of PtPd nanostructures [24, 32]. Fig. 2 compares the surface at the edge and center area of a 16 cm^2 PtNW GDE and PtPd GDE with 5 at% Pd. It can be seen that the distribution of PtPd nanostructures has much less difference at the edge and in the center area as compared to Pt.

8

Although the PtPd nanodendrites have been reported by many groups, including both in solutions [23, 28, 33] and on supports, e.g. on graphene [32, 34], the growth mechanism was all simply inferred based on the standard reduction potential. There is really not a lot of evidences for the crystal growth mechanism. To help clear this point, in this work, the time-dependent in-situ growing process was analysed for PtPd GDE with 5 at% Pd. The reaction solution from 0 to 92 hours was monitored by UV-Vis spectroscopy to evaluate qualitatively the remained metal ions which haven't been reduced by formic acid. The absorption spectrum lines of the Pd and Pt precursors as well as that of the PtPd mixture at different time intervals are shown in Fig. S1. The results indicate that the reduction of Pd mainly happens at the initial stage of the reaction and nearly all Pd ions are reduced in the first 2 hours, but the whole reaction, in particular the reduction of Pt will not finished until 24 hours later.

To further understand the crystal growth mechanism, the morphological evolution of PtPd nanostructure with 5 at% Pd on the GDL surface at various reaction periods were examined by TEM with EDX analysis (Fig. S2). The results show a very high Pd ratio in the beginning, followed by a fast dropping to a quite low level, suggesting that PtPd alloy nanoparticles with a dominated amount of Pd at the initial stage are formed at first, which are then working as seeds for the following growth to nanodendrites. The branches of nanodendrites are dominated by Pt due to most Pd has been reduced in the initial period in nanoparticle formation. These changes are consistent with that shown by UV-Vis spectra. The branch diameter of the as-obtained nanodendrites is ca. 4 nm, and the length is ca. 5–20 nm. The crystalline nature of final PtPd nanodendrites was elucidated by the selected-area electron diffraction

9

(SAED) pattern, and intense rings can be assigned to the (111), (200), (220) and (311)

planes of the Pt face-centred cubic (fcc) crystals (inset in Fig. 3a). A HR-TEM image

shown in Fig. 3b displays typical nanodendrites. The inset image indicates a lattice

spacing distance of 0.22 nm for one branch of PtPd nanodendrites, which is slightly

smaller than 0.23 nm of the {111} lattice spacing of the bulk Pt. This contraction of

lattice caused by the addition of Pd is in line with the reported results in literature [35],

which indicates the interactions between Pt and Pd atoms in the formed PtPd NDs.

The fast reduction of Pd and their role as growing seeds on GDL surface indicates a

non-negligible influence of the amount of Pd on the formation of the final

nanostructures. Some early researches have been carried out by other groups to this

synthesis for supported and un-supported catalysts [24, 28, 33]. But, all of them only

focus on the pure material research, and none of them has demonstrated the real

catalytic performance of these nanostructures in practical fuel cells. In particular,

when this synthesis is conducted directly on the large-area GDL surface, the effect of

Pd is thus different from that in solution or supported-catalysts. Fig. S3 shows TEM

images of PtPd nanostructures with various Pd atomic contents. At a high Pd content

of 50 at%, a high supersaturation of Pd atoms greatly lowers the free-energy barrier

for heterogeneous nucleation and is responsible for the rapid nucleation rate of Pt with

a vanishingly small growth rate [36]. Therefore, the main morphology obtained is

spherical PtPd nanoparticle aggregate with an average particle size of ca. 5 nm (Fig.

S3a). But, when pure Pd is used, rather than Pd nanoparticles obtained as those

reported in literature [31, 33, 34], very large Pd crystal grains are observed (Fig. S3e

and f). In one case, this indicates the important effects of the existing of Pt ions with

Pd in the formation of nanoparticles on the GDL surface, as that with 50 at% Pd. On

the other hand, it suggests different crystal growth mechanisms on the large-area GDL as compared with those in solution or on supports. With the decrease of the Pd content, the nucleation sites provided are reduced, and accordingly, short nanodendrites (Fig. S3b) are formed through the reported particle attachment growth process [28]. Decreasing the Pd content to 10 at%, a high yield of nanodendrites is obtained. The branch shows a length of ca. 5–10 nm (Fig. S3c). With a further decrease in Pd, PtPd nanodendrites with longer and dense branches are obtained (i.e. Fig. 3 at 5 at%). At 2.5 at% Pd, the branch length increases to 10–20 nm (Fig. S3d). Therefore, in the presence of a high Pd content nanoparticles are inclined to form, and nanodendrites are achieved when the Pd content decreases.

To further understand the crystal structure of the as-prepared PtPd nanostructures, XRD analysis was performed to the plain GDL 35BC, GDEs of Pt, Pd and PtPd 5 at% (Fig. S4). PtPd 5 at% NDs show the characteristic peaks locating between single Pt (JCPDS-04-0802 Pt) and Pd (JCPDS-46-1043 Pd) [37, 38], indicating the formation of the solid-solution PtPd alloy again, as supported by the HRTEM results (Fig. 3b). The much stronger intensity of the Pd peaks also confirms the very large crystal grains formed (Fig. S3e and f). XPS analysis was conducted to identify near-surface species involved in PtPd heterostructures (Fig. S5). It can be seen that, with the increase of Pd, the intensity of Pd 3d peaks becomes stronger while that of the Pt 4d peaks becomes weaker, and all peaks shift more positively compared with the monometallic Pt (4d3/2 at 331.6 eV) and Pd (3d5/2 and 3d3/2 at 335.2 and 340.5 eV, respectively), suggesting the PtPd interactions [39] change the atomic structure thus contributing to the enhanced activity in PtPd bimetallic hybrids [31].

In order to understand the influence of Pd content on the catalytic performance of PtPd nanostructures in real fuel cell conditions, PtPd GDEs fabricated with different Pd contents were directly used as cathodes and tested in 16 cm^2 hydrogen-air PEFCs. Cathode CVs were recorded in-situ in single cells to measure the electrochemical active specific area (ECSA) of catalysts within electrodes. From CVs in Fig. 4, normalized by the metal loading in precursors (checked by TGA shown in Fig. S6), ECSAs for PtPd GDEs with Pd atomic percentages of 50, 25, 10, 5, 2.5 and 0.5, as well as PtNW GDE are 0.49, 7.21, 11.59, 22.40, 18.76, 18.15 and 14.70 m^2 g^{-1}, respectively. The smallest ECSA value of PtPd 50 at% GDE can be ascribed to the nanoparticle aggregates formed on the GDL surface (Fig. S3a). This aggregation reduces contribution of catalysts to the three-phase boundary (TPB) in the electrodes and leads to a low catalyst utilisation ratio in fuel cell electrode [40]. Larger ECSA is obtained as aggregates reduce with a decreased Pd content. When the composition of Pd arrives at 5 at%, a larger ECSA is achieved as expected due to the more regular PtPd NDs achieved. The ECSA of PtPd 2.5 and 0.5 at% GDEs are slightly lower, which can be ascribed to the longer and denser nanodendrite branches (Fig. S3d) and their relative non-uniform distribution on GDLs (Fig. 2a and b). With a similar morphology, the larger ECSA of PtPdND GDEs at the low Pd content than that of PtNW GDE indicates that PtPdND GDE is more electrochemically accessible due to their better distribution on the GDL surface. However, the anisotropic morphology still results in a much lower ECSA for the PtPd ND GDE as compared to the commercial Pt/C nanoparticle catalysts (30.91 m^2 g^{-1}), which is in line with those reported in literature [10,29].

Fig. 5 shows polarization curves and their power densities at 0.6 V of the MEAs with the as-prepared PtPd GDEs, as well as PtNW and Pt/C GDEs. The comparison is conducted at 0.6 V because this is the common voltage used in practical operational conditions of PEFCs. Although a much larger ECSA is observed for Pt/C nanoparticles, the power performance obtained is much lower, and the power density at 0.6 V is only 0.55 W cm^{-2}, while PtNW GDE exhibits a higher value of 0.64 W cm^{-2}. Regarding PtPd GDEs, at a high Pd amount, e.g. 50%, the lower catalyst utilisation ratio from the aggregated nanoparticles finally results in a poor electrode performance. With decrease of the Pd content, a better performance is obtained, reaching the maximum value at 5 at%. At this optimal Pd content, the uniform distribution of NDs enables a more porous catalyst layer, which facilitates oxygen diffusion to the catalyst surface to achieve a reduced mass transfer loss and a higher catalyst utilization ratio, thus a better catalytic performance is expected. Further decrease of the Pd content leads to PtPd NDs with longer and dense branches, as well as the relative non-uniform distribution on GDL surface (Fig. 2 and S3), finally resulting in a lower catalyst utilization ratio and thus a decline of the electrode performance. The power performance of PtPdND GDE with 5 at% Pd exhibits the highest power density of 0.73 W cm^{-2} at 0.6 V, better than those of both PtNP/C and PtNW GDEs, demonstrating the advantages from both the 1D morphology over the 0D nanoparticles and the PtPd hybriding over pure Pt nanowires.

To further understand the effect of the behaviour of PtPd nanostructures on power performance, EIS measurements were conducted at three current densities for PtPd GDEs with different compositions as well as to the Pt/C and PtNW GDEs (Fig. 6). At a low current density of 0.05 A cm^{-2}, the impedance represented by the diameter of

13

the semi-circle is mainly contributed by charge transfer resistance, indicating ORR catalytic kinetic performance. Fig. 6a shows the largest impedance with the PtPdND GDE with 50 at% Pd. The smallest semicircle is observed for the PtPd GDE with 5 at% Pd, indicating the lowest charge transfer resistance and thus the best ORR catalytic kinetic performance. However, all PtPd GDEs with medium and low Pd contents together with Pt/C and PtNW GDEs show similar impedances, implying a close ORR catalytic kinetic performance for all of them. This is slightly different from those reported higher catalytic activities from the enhanced effect of PtPd over Pt by the measurement conducted in liquid electrolytes [20]. Although the clear mechanism is still not clear now, it can possibly ascribed to the much complex test environment in practical fuel cells compared with that in the liquid electrolyte. Here, besides the intrinsic catalytic activities, the catalyst behaviour and their surrounding environment in electrode together determine the final performance in fuel cells. With the increase of the current density (Fig. 6b and c), the 2nd semicircle appears on EIS which mainly represents mass transfer resistance within electrodes. PtPdND GDE with 5 at% Pd still shows the smallest charge and mass transfer resistance, while the GDEs with Pt/C nanoparticles and PtPd GDE 50 at% exhibit very large resistances due to their dense electrode structure. These EIS measurement results demonstrate the much reduced mass transfer loss in the PtNW GDE as compared with those from both PtPd and Pt nanoparticles, and a further improvement can also be achieved by introducing a small amount of Pd to optimise their distribution on GDL surface.

Besides catalytic activities, a high stability is also usually reported for PtPd hybrid structures over Pt [41], which is based on the enhanced effect of Pd and Pt preventing the dissolution of catalysts during the potential cycling. To check the effect of

14

introducing Pd to the as-prepared PtPd NDs on the GDE performance in fuel cells, an accelerated degradation test (ADT) was carried out by 3000 potential sweeping cycles in the single cell at room temperature. Cathode CVs after the ADT test are displayed with the initial curves and compared with those of PtNWs and Pt/C nanoparticles in Fig. 7a. After the ADT, all GDEs exhibit a big decline of their ECSAs, and a lower ratio is observed to the PtPdND GDE as compared with PtNW one, which agrees well with those reported in literature [37, 38], but the one from Pt/C shows the least drop. The remaining values of PtNW, PtPdND and Pt/C GDEs are 5.55, 11.96 and 21.25 m^2 g^{-1}, corresponding to 62.2%, 46.6% and 31.2% loss of their initial ECSAs, respectively (Fig. 7c). Fig. 7b shows polarization curves for all GDEs after the ADT. It can be seen that the PtPdND GDE still exhibits a higher power performance than the PtNW GDE at 0.6 V, and the Pt/C GDE shows a very low performance, corresponding to degradation ratios of 19.9%, 12.7% and 27.5% (Fig. 7d), respectively. At the high voltage region (>0.7V), PtNW GDE presents a higher power performance, indicating a better kinetic activity than PtPdND GDE, which can be explained by the higher mass activity remained after the ADT [11,40]. The larger ratio of ECSA loss than the lower degradation percentage of power performance indicates the increase in the specific area activity of catalysts [42], and the result shown here indicates this improvement becomes larger with the increase of the aspect ratio from nanoparticles, NDs to NWs. Although the detailed mechanisms are still not clear at the moment [1], this phenomenon further demonstrates advantages of 1D nanostructured catalysts for PEFC applications.

4. Conclusions

In summary, we have demonstrated a catalyst electrode from PtPd nanodendrites in-situ grown on large-area gas diffusion layer carbon paper surface by a facile wet chemical procedure. The experimental results show that the content of Pd greatly influences the final morphology and distribution of PtPd nanostructures on GDL surfaces, which together determines the final power performance in PEFC applications. The introducing of an optimal amount of Pd, i.e. 5 at% to Pt nanowire growth leads to more uniform distributed PtPd nanodendrites on the GDL surface, reducing the mass transfer resistance within the electrode to achieve a high power performance. Besides, PtPd NDs exhibit a higher power performance over Pt NWs even after the durability test in PEFCs, showing a lower loss of ECSA but a higher degradation percentage of power performance. Due to an analogous catalyst electrode could be formed based on other hybrid anisotropic nanostructures, the results here point to new electrode preparation strategies that leverage both the catalyst intrinsic activity and the electrode structure for high performance PEFCs.

Supporting Information

Supporting information includes additional information on the UV-Vis spectra, EDX analysis results, SEM images of Pd grown on GDL, TGA curves and a comparison of polarization curves of PtPd GDE fabricated by two growing procedures.

References

[1]   C. Koenigsmann, S.S. Wong, Energ Environ Sci 4 (2011) 1161-1176.

[2]   G. Zhang, S. Sun, M. Cai, Y. Zhang, R. Li, X. Sun, Sci Rep 3 (2013) 1526.

[3]   S. Sun, G. Zhang, D. Geng, Y. Chen, R. Li, M. Cai, X. Sun, Angewandte Chemie Int Ed 50 (2011) 422-426.

[4]   S.M. Alia, G. Zhang, D. Kisailus, D. Li, S. Gu, K. Jensen, Y. Yan, Adv Funct Mater 20 (2010) 3742-3746.

[5]   B.Y. Xia, W.T. Ng, H.B. Wu, X. Wang, X.W. Lou, Angew Chem Int Ed 51 (2012) 7213–7216.

[6]   L.Y. Ruan, E.B. Zhu, Y. Chen, Z.Y. Lin, X.Q. Huang, X.F. Duan, Y. Huang, Angew Chem Int Edit 52 (2013) 12577-12581.

[7]   S. Du, Int J Low-Carbon Tech 7 (2012) 44-54.

[8]   S. Sun, G. Zhang, D. Geng, Y. Chen, M.N. Banis, R. Li, M. Cai, X. Sun, Chem –Eur J 16 (2010) 829-835.

[9]   S.F. Du, J. Power Sources 195 (2010) 289-292.

[10]   S.F. Du, K.J. Lin, S.K. Malladi, Y.X. Lu, S.H. Sun, Q. Xu, R. Steinberger-Wilckens, H.S. Dong, Sci Rep 4 (2014) 6439.

[11]   Y.X. Lu, S.F. Du, R. Steinberger-Wilckens, Appl Catal B-Environ 164 (2015) 389-395.

[12]   X.Y. Yao, K.H. Su, S. Sui, L.W. Mao, A. He, J.L. Zhang, S.F. Du, Int J Hydrogen Energ 38 (2013) 12374-12378.

[13]   L. Su, S. Shrestha, Z. Zhang, W. Mustain, Y. Lei, J Mater Chem A 1 (2013) 12293-12301.

[14] I.E.L. Stephens, A.S. Bondarenko, U. Gronbjerg, J. Rossmeisl, I. Chorkendorff, Energ Environ Sci 5 (2012) 6744-6762.

[15] J. Greeley, I.E.L. Stephens, A.S. Bondarenko, T.P. Johansson, H.A. Hansen, T.F. Jaramillo, J. Rossmeisl, I. Chorkendorff, J.K. Norskov, Nat Chem 1 (2009) 552-556.

[16] Y.H. Bing, H.S. Liu, L. Zhang, D. Ghosh, J.J. Zhang, Chem Soc Rev 39 (2010) 2184-2202.

[17] W.T. Yu, M.D. Porosoff, J.G.G. Chen, Chem Rev 112 (2012) 5780-5817.

[18] C. Koenigsmann, S.S. Wong, ACS Catal 3 (2013) 2031-2040.

[19] Y.J. Deng, N. Tian, Z.Y. Zhou, R. Huang, Z.L. Liu, J. Xiao, S.-G. Sun, Chem Sci 3 (2012) 1157-1161.

[20] H. Zhang, M.S. Jin, Y.N. Xia, Chem Soc Rev 41 (2012) 8035-8049.

[21] Z. Zhu, Y. Zhai, C. Zhu, Z. Wang, S. Dong, Electrochem Commun 36 (2013) 22-25.

[22] S.M. Alia, K.O. Jensen, B.S. Pivovar, Y. Yan, ACS Catal 2 (2012) 858-863.

[23] B. Lim, M. Jiang, T. Yu, P.C. Camargo, Y. Xia, Nano Res 3 (2010) 69-80.

[24] S. Ghosh, S. Mondal, C. Retna Raj, J Mater Chem A 2 (2014) 2233-2239.

[25] Y.Z. Lu, Y.Y. Jiang, W. Chen, Nano Energy 2 (2013) 836-844.

[26] C. Zhu, S. Guo, S. Dong, Adv Mater 24 (2012) 2326-2331.

[27] S.J. Guo, S.J. Dong, E.K. Wang, Chem Commun 46 (2010) 1869-1871.

[28] J.-J. Lv, J.-N. Zheng, S.-S. Li, L.-L. Chen, A.-J. Wang, J.-J. Feng, J Mater Chem A 2 (2014) 4384-4390.

[29] S.H. Sun, F. Jaouen, J.P. Dodelet, Adv Mater 20 (2008) 3900-3904.

[30] S.H. Sun, D.Q. Yang, D. Villers, G.X. Zhang, E. Sacher, J.P. Dodelet, Adv Mater 20 (2008) 571-574.

[31] S. Du, Y. Lu, R. Steinberger-Wilckens, Carbon 79 (2014) 346-353.

[32] X. Chen, Z. Cai, X. Chen, M. Oyama, J Mater Chem A 2 (2014) 315.

[33] L. Wang, Y. Yamauchi, Chem-Asian J 5 (2010) 2493-2498.

[34] S.J. Guo, S.J. Dong, E.K. Wang, ACS Nano 4 (2010) 547-555.

[35]   Y. Kim, Y. Noh, E.J. Lim, S. Lee, S.M. Choi, W.B. Kim, J Mater Chem A 2 (2014) 6976-6986.

[36]   A. Cacciuto, S. Auer, D. Frenkel, Nature 428 (2004) 404-406.

[37]   X. Yang, Q.D. Yang, J. Xu, C.S. Lee, J Mater Chem 22 (2012) 8057-8062.

[38]   Y.C. Tseng, H.S. Chen, C.W. Liu, T.H. Yeh, K.W. Wang, J Mater Chem A 2 (2014) 4270-4275.

[39]   C.Z. Zhu, S.J. Guo, S.J. Dong, Adv Mater 24 (2012) 2326-2331.

[40]   H.A. Gasteiger, S.S. Kocha, B. Sompalli, F.T. Wagner, Appl Catal B-Environ 56 (2005) 9-35.

[41]   L.X. Ding, C.L. Liang, H. Xu, A.L. Wang, Y.X. Tong, G.R. Li, Adv Mater Interfaces (2014) 1400005.

[42]   P. Hernandez-Fernandez, F. Masini, D.N. McCarthy, C.E. Strebel, D. Friebel, D. Deiana, P. Malacrida, A. Nierhoff, A. Bodin, A.M. Wise, J.H. Nielsen, T.W. Hansen, A. Nilsson, I.E.L. Stephens, I. Chorkendorff, Nat Chem 6 (2014) 732-738.

Figure captions:

Fig. 1 Illustration of fuel cell setup.

Fig. 2 SEM images of (a, b) PtNW GDE and (c, d) PtPd GDE with 5 at% Pd. (a, c) and (b, d) show the edge and center area of the two GDE pieces, respectively.

Fig. 3 TEM images of PtPd nanostructures with 5 at% Pd in-situ grown on GDL surface. Insets in (a) and (b) show the SAED pattern and HR-TEM image of one branch, respectively.

Fig. 4 Cathode CVs for GDEs from Pt/C, PtNWs and PtPdNDs with different compositions.

Fig. 5 (a) Polarization curves and (b) the trend of the power density at 0.6 V for PtPd GDEs with different Pd contents and PtNW and Pt/C GDEs.

Fig. 6 EIS measured at (a) 0.05, (b) 0.5 and (c) 1.0 A cm^{-2} for PtPdND GDEs with various Pd contents, PtNW and Pt/C GDEs.

Fig. 7 (a) CVs, (b) polarization curves, (c) ECSAs and (d) power densities at 0.6 V for GDEs from PtPdNDs with 5 at% Pd, PtNWs and Pt/C nanoparticles before and after the ADT test.